Ammonia emissions from a dairy housing and a wastewater treatment plant quantified with an inverse dispersion method accounting for deposition loss

Alex C. Valach[1*], Christoph Häni[1], Marcel Bühler[1,2], Joachim Mohn[3], Sabine Schrade[4], and Thomas Kupper[1]

[1] School of Agricultural, Forest and Food Sciences, Bern University of Applied Sciences, Switzerland
[2] Department of Biological and Chemical Engineering, Aarhus University, Denmark
[3] Laboratory for Air Pollution/Environmental Technology, Empa Dübendorf, Switzerland
[4] Ruminant Nutrition and Emission, Agroscope Tänikon, Switzerland

*corresponding author:
alex.valach@bfh.ch

Keywords:

Ammonia emissions; inverse dispersion method; backward Lagrangian stochastic model; miniDOAS; wastewater treatment; cattle housing

Abstract

Ammonia (NH_3) emissions negatively impact air, soil, and water quality, and thus human health and biodiversity. A large share of emissions, including the largest sources, originate from single or multiple source structures, such as livestock facilities, but also wastewater treatment plants (WWTPs). The inverse dispersion method (IDM) has proven to be effective in measuring total emissions from such structures, however depositional loss between the source and point of measurement is not always accounted for. We applied IDM with a deposition correction to determine total emissions from a representative dairy housing and WWTP during several months in autumn and winter in Switzerland. Total emissions were 1.19 ± 0.48 and 2.27 ± 1.53 kg NH_3 d^{-1} for the dairy housing and WWTP, respectively, which compared well with published emission data for the respective seasons, albeit very few comparable studies exist for WWTPs. A concurrent comparison with an inhouse tracer ratio method at the dairy housing indicated an underestimation of the IDM results by <20%. Diurnal emission patterns were evident at both sites likely driven by changes in air temperature and to a lesser extent wind speed, but possibly also indicating lagged effects of management activities such as sludge tank agitation at the WWTP. Modelled deposition corrections to adjust the concentration loss detected at the measurement point with the associated footprint were 22-28% of the total emissions and the cumulative fraction of deposition to emission modelled with distance from the source was between 7-9% and 9-12% during unstable and stable meteorological conditions, respectively, for the given measurement distances of 60-150 m. Although estimates of depositional loss were plausible, the approach is still connected with substantial uncertainty, which calls for future validation measurements. Longer measurement periods encompassing more management activities and ranges of environmental conditions across all seasons are required to assess the effect of predictor variables on emission dynamics. Combined, IDM with deposition correction will allow the determination of emissions factors at reduced efforts and costs and thereby support the development and assessment of structural and operational emission reducing technologies and enlarge the data availability for emission inventories.

Introduction

Ammonia (NH_3) emissions have detrimental effects on soils and aqueous ecosystems via acidification, eutrophication, and subsequent loss of biodiversity but also on air quality due to the formation and growth of particulate matter which impacts human health (Sutton et al. 2011; Fowler et al. 2015; Galloway et al. 2021). Agriculture and more specifically, the livestock sector is the largest emitter of NH_3 with 80-85% globally and approx. 90% in Switzerland (Kupper et al. 2015; van Damme et al. 2021). Especially in countries with high livestock densities, animal housing and manure application are primary sources. Other point sources include wastewater treatment plants (WWTPs), of which there are many smaller plants distributed in Switzerland.

Traditionally, NH_3 emissions from naturally ventilated dairy housings are quantified by combining concentration measurements in the housing with the ventilation rate (Calvet et al. 2013). Many studies have measured NH_3 emissions from dairy housings and calculated emission factors are used to normalise emissions by animal taking different climatic conditions into account (Flesch et al. 2009; Schrade et al. 2012; Hempel et al. 2016). However, difficulties remain when comparing these emissions due to the significant effects of differences in housing types, management and measurement methods (Poteko et al. 2019), but also the timing and duration of measurements (Kafle et al. 2018). For example, loose housings with natural ventilation are the prevalent dairy housing system in western Europe (Sommer et al. 2013), yet annual mean emissions even standardised by livestock unit (LU = 500 kg live weight) vary by orders of magnitude between 3.4 g NH_3 LU^{-1} d^{-1} to 98.4 g NH_3 LU^{-1} d^{-1} (Wu et al. 2012; Poteko et al. 2019) depending on the climate and farm conditions during the measurements, as well as the measurement method employed. Schrade et al. (2012) measured NH_3 emissions from six dairy loose housings with outdoor exercise areas in Switzerland using a tracer ratio method resulting in means between 6 and 67 g NH_3 LU^{-1} d^{-1} throughout the year. Although this method is considered state-of-the-art, it has limited applicability for farm-scale measurements due to its extensive experimental setup (Mendes et al. 2015). Generally, the method is easier for single structures as it must be carefully tailored to scale with the source strength in the case of multiple or inhomogeneous sources. Although small quantities are used, the frequently used tracer, sulphur hexafluoride (SF_6), is the most potent and extremely long-lived greenhouse gas falling under the F-Gas Regulation in Europe (EU Directive EC No 842/2006 a).

Although only a marginal source albeit with high uncertainties in the national emissions inventory, WWTPs represent a similar source configuration and measurement difficulties for NH_3 emissions as dairy housings (Kupper et al. 2013; Samuelsson et al. 2018). Generally, emissions are poorly quantified worldwide due to their spatial arrangement and temporal variations. In Switzerland, 64% of WWTPs are small to medium-sized (processing wastewater from <10000 inhabitants each). They treat only 20% of the total amount of wastewater, while the largest nine WWTPs process 25% of the total sewage volume (Abegglen and Siegrist 2012). The sludge line is expected to be the major source of NH_3, although there is a paucity of data on whole plant and individual source emissions. It often comprises thickening of primary and excess sludge, anaerobic treatment in a digester, and subsequent storage of the anaerobically stabilised liquid sludge. Optionally, the sludge can be dewatered and stored before disposal. For storage of liquid sludge in open tanks, emission peaks are expected due to regular agitation for further transport and processing. Samuelsson et al. (2018) estimated total emissions of 4.3 g NH_3 PE^{-1} yr^{-1} for a plant with 805000 person equivalents (PE) in Sweden, of which 66% likely originated from the sludge line. Sutton et al. (1995a) estimated up to 27 g NH_3 PE^{-1} yr^{-1} for a medium-sized facility (165000 PE) relying on several assumptions. Upscaled emissions from laboratory studies on wastewater (means of 3.2 g NH_3 m^{-2} h^{-1}) or even different livestock manures can be a further source for emissions data (Dai et al. 2015).

Measuring gas emissions from open structures is challenging due to the source configuration and scale, as emissions are heterogeneous and dynamic in space and time (Bühler et al. 2022). The inverse dispersion method (IDM) combines line-integrated concentration measurements up- and downwind of the source with results from modelling the inverse dispersion of the plume, such as from a backward Lagrangian stochastic (bLS) model. This method has been successfully applied to estimate emissions from whole farms, including animal housings (Flesch et al. 2005; Flesch et al. 2007; Flesch et al. 2009; Harper et al. 2010), feedlots (Flesch et al. 2007; McGinn et al. 2007; McGinn et al. 2016), and manure stores (Flesch et al. 2013; Grant et al. 2013; Baldé et al. 2018). In a controlled methane release experiment in a barn Gao et al. (2010) achieved a recovery rate, i.e. the fraction of the modelled release rate to the emitted trace gas, of 0.93-1.03 using this method. The micrometeorological assumptions include constant wind speeds, large fetch, and homogeneous terrain, as well as an emission plume that is clearly distinguished from ambient concentrations. The latter is particularly challenging for Switzerland, where smaller but very densely dispersed emission sources from farms with an average size of 22 dairy cows (Federal Statistical Office 2020) result in weaker emission plumes and high background levels. Despite this and the sometimes non-ideal terrain conditions, we previously demonstrated the effective application of IDM to quantify methane emissions under these constraints by optimising the filtering criteria (Bühler et al. 2021; 2022). The optimised method yielded a good comparability with an inhouse tracer ratio method (iTRM) as a reference (Mohn et al. 2018) with differences in methane emissions of 1 - 8%, which were well within the uncertainty range of both methods (i.e., <10% for tracer ratio and <24% for IDM (Mohn et al. 2018; Bühler et al. 2021)). The description inhouse for iTRM refers to the release of a tracer gas inside of the housing.

An underlying assumption of bLS models is that the analysed gas is inert, which is satisfied for methane but not necessarily for NH_3. Ammonia is very reactive and soluble with a high affinity to adsorb to surfaces and thus experiences greater losses mostly by deposition (Loubet et al. 2009; Schrader and Brümmer 2014). As a general rule, 20-25% of total NH_3 and ammonium (NH_4^+) is expected to deposit within 1 km of the source, 50-60% within around 2-4 km and the rest depositing within 10-50 km (Asman and van Jaarsveld 1992; Asman 1998; Sutton et al. 1998; Loubet et al. 2006; Loubet et al. 2009). Measurements from pig farms showed deposition losses up to 6% within 500 m (Bajwa et al. 2008), but

Loubet et al. (2017) found that the cumulative deposition within only 200 m downwind on a fertilised grassland site ranged from 4% to 34% and therefore may not always be negligible. Deposition distances vary strongly with source height and depend on wind speed, atmospheric stability, surface resistance and roughness, as well as load compensation points. The latter especially affects the initial loss between the source area and the point of measurement that is dominated by dry deposition, hence relevant for IDM (Loubet et al. 2009). Likewise, modelling studies have estimated that in total about 44% of emitted NH_3 is lost in the vicinity of the source area through dry deposition of gaseous NH_3, while NH_4^+ aerosols travel longer distances (Asman et al. 1998). Although line-integrating instruments are located 100-150 m from the source, the deposition loss is often not accounted for in emission measurements, which leads to a systematic underestimation when determining total emissions from defined hot spots or source areas (Häni et al. 2018).

The aim of this study was to 1) determine emission estimates for building-scale sources in different emission sectors (i.e., dairy housing and WWTP) as reported for the Swiss NH_3 emissions inventory using measurements over several weeks to months, 2) apply IDM accounting for dry deposition losses to determine total emissions of building-scale NH_3, 3) compare NH_3 emissions by IDM with iTRM for the dairy housing, and 4) estimate the impact of depositional losses for the given IDM instrument setups. Here we present measurements from a dairy loose housing and the first facility-scale measurements of NH_3 emissions from a representative WWTP in Switzerland.

Methods

2.1 Site descriptions

2.1.1 Loose dairy housing

Measurements were conducted at an experimental loose housing for dairy cows in Aadorf, Switzerland (47.489175° N, 8.919663° E, 544 m altitude) (Mohn et al. 2018). The building is naturally ventilated with the long axis positioned perpendicular to the prevailing wind directions (NE and SW) for optimal ventilation. While the building itself is situated on a flat plain extending >1 km to the SW, the surrounding topography consists of a descending slope (9% over 50 m height difference) 220 m to the NE, a small forest 200 m west and several buildings and trees (<15 m height) to the north, as well as other livestock housings beyond a radius of 250 m but within 600 m, plus surrounding pastures with grazing cattle and sheep (Figure 1).

The housing consists of two compartments for 20 cattle each with straw mattress cubicles and a solid floor covered by a rubber mat (KURA P, Gummiwerk KRAIBURG GmbH, Tittmoning, Germany). The milking and waiting area were situated between the compartments along with other technical installations and an office. Each housing compartment was equipped with a cross channel which ran perpendicular to the building's long axis and led to an adjacent underground slurry store to the west of the housing and was separated by rubber flaps. The slurry store consisted of two compartments of 252 m^3 in total with a solid cover and four openings. The housing compartments were not thermally insulated. Ventilation was adjusted with flexible curtains along façades, which during the measurement periods were varied from completely open, through a combination of completely closed on the NE side and partially or completely closed on the SW side, to completely drawn on all sides. The curtains were fully closed for the last four days of the first measurement period and during the entire second measurement period. More information on the study site can be found in (Poteko et al. 2018; Bühler et al. 2021).

Management routines included milking twice daily (05:30 and 16:30 local time), as well as dung removal with stationary scrapers 12 times per day. During the measurements 40 primiparous and multiparous lactating Brown Swiss and Swiss Fleckvieh cows were housed in the building. The diets of the dairy cows consisted of a mixture of maize and beans, or grass silage, maize silage and hay supplemented with concentrates being individually allocated by an automatic feeder according to milk yield and lactation stage. The average body weight was 701 kg in autumn and 685 kg in winter with a mean daily milk yield of 23.2 kg and 25.7 kg, respectively. The cows had no access to the pasture or outdoor exercise areas during the experiment.

2.1.2 Wastewater treatment plant

Measurements were conducted at a medium-sized WWTP (47.055620° N, 7.539515° E, 507 m altitude) which used a conventional activated sludge treatment with complete nitrification and denitrification. The plant processed waste of 43534 PE, which corresponded to 33126 connected inhabitants plus industrial waste. The site encompassed an area of 2.18 ha and consisted of multiple emitting structures including sand traps, primary and secondary clarifiers, activated sludge tanks, thickener and digester towers (total volume of 2200 m^3), a gas storage tank and open sludge storage tanks. It was selected based on the suitability of the location for IDM measurements i.e., minimal topographic obstructions (Figure 2). No large undulations or additional emission sources were present within 1 km in the dominant wind direction (SW). The plant applied conventional activated sludge treatment with complete nitrification and denitrification. The thickened sludge had a dry matter content of 4% before entering the anaerobic digester where it resided for 20 days. It was then further dewatered again to 8% dry matter content through the addition of flocculants by means of a rotary screen. Afterwards the sludge was stored in open tanks with a total volume of 1960 m^3 (632 m^3 in use at the time) and a surface of 331 m^2, which were regularly agitated typically in the morning before part of the sludge was transported to another facility for further treatment and incineration. Mean operational data during the measurement period were comparable to annual means (see Table SI2.1 for average operational data during the measurement periods). The mean incoming N load from ammonium (NH_4-

N) during the measurement period was 350 kg NH_4-N d^{-1} in total or 7.8 g NH_4-N PE^{-1} d^{-1} which is within the expected range for Swiss WWTPs (Kupper and Chassot, 1999).

2.2 Measurement campaigns

Measurements at the dairy housing were split into two periods of 36 days (autumn) and 23 days (winter) from September to December 2018, but only one measurement period at the WWTP lasting 21 days from late September to mid-October 2019. Ammonia concentrations were measured using miniDOAS instruments placed up- and downwind of the emission sources (Figures 1 and 2). The instruments are open-path optical devices which measure line-integrated gas concentrations between a light source and detector by UV absorption (200-230 nm wavelengths) (see Sintermann et al. 2016 for more details). The path length, here 50 m, is determined by the placement of the reflectors and the miniDOAS, which houses both the light source and detector in an environmentally controlled container. Downwind instruments were placed at a distance of approx. 10 times the maximum building height (i.e., the dairy housing was 8.5 m and the WWTP up to 15 m high) to avoid wind flow disturbance by the structures (Harper et al. 2011). At the dairy housing one set of instruments was placed 120 m NE of the building, while the second set was around 60 m SW due to topographic restrictions, while at the WWTP the up and downwind placements were 100 – 150 m.

The iTRM measurements at the dairy housing were conducted as a comparison and consisted of 2 measurements lasting 4 or 8 days during each measurement period. The measurement principle of the dual tracer ratio method is described in Mohn et al. (2018) and consisted of dosing each housing compartment with a different tracer gas (i.e., sulphur hexafluoride (SF_6) and trifluoromethyl sulphur pentafluoride (SF_5CF_3)) to identify emissions from each location. Then the tracer and target (NH_3) gas concentrations are concurrently quantified at a point outside of the housing using a Picarro analyser (G2301, Picarro Inc., USA) to calculate the resulting emissions based on the ratio of the background-corrected gas concentrations of each target to tracer gas and the dosed mass flow of the tracer gases. This method assumes that the dispersion of the tracer gas behaves the same way as the target gas and mimics its emissions. Background concentrations were sampled 30 m SE of the housing (Figure 1). The exact setup and data processing is described in Mohn et al. (2018). The iTRM data provided average emissions for 10 min intervals for each compartment, which were summed and then averaged to 30 min means before being compared with the corresponding 30-min IDM measurement intervals.

Three-dimensional sonic anemometers (Gill Windmaster, Gill Instrument Ltd., Lymington, Hampshire, UK) were installed up- and downwind of the source structures at around 1.4 m height to measure the wind flow and turbulence for the bLS model and logged at 10 Hz. Since the wind direction at the dairy housing alternated between SW and NE, only data from the respective downwind sonic was used for bLS model. Additional meteorological data (air temperature, pressure, precipitation) were obtained at both sites using an OTT WS700 weather station (OTT Hydromet GmbH, Germany) and at the dairy housing a nearby weather station (Tänikon, MeteoSwiss) provided additional meteorological data. Coordinates of the instruments and source locations are needed for the bLS model and were collected with a handheld GPS (Trimble Pro 6T, Trimble Navigation Limited, Westminster, USA). At both sites methane was also measured and the results were published in Bühler et al. (2021; 2022).

2.3 Inverse dispersion modelling

Inverse dispersion modelling is a micrometeorological method to determine gaseous emissions in a downwind plume from sources of a known dimension and spatially constrained area. The concentration difference ΔC (mg m^{-3}) between background levels in upwind C_{BG} and downwind C_{DW} measurements of a source is combined with the bLS model based on the measured turbulence characteristics to calculate the dispersion factor D_{bLS} (s m^{-3}) needed to estimate an emission flux Q (eq. 1).

$$Q = \frac{C_{DW} - C_{BG}}{D_{bLS}} \qquad \text{(eq. 1)}$$

The bLS model based on (Flesch et al. 2004), which is a surface layer model covering distances <1 km, was used to calculate the dispersion factor (eq. 2) from the total backward trajectories of the line-integrated concentration measurements. The measurement path was approximated by a series of points spaced 1 m apart and propagated backward to the source area and hence is proportional to the ratio of the simulated concentration to the emission rate $(C/E)_{bLS}$ as follows,

$$D_{bLS} = \frac{(C/E)_{bLS}}{A_{source}} = \frac{1}{N_{Traj}} \sum_{TD_{inside}} \left(\frac{2}{w_0}\right) * \frac{1}{A_{source}} \qquad \text{(eq. 2)}$$

For each point and measurement interval, 250000 backtrajectories were calculated and analysed for touchdowns (TD_{inside}) within the source area (A_{source}), which provide the touchdown location coordinates and vertical velocity (w_0).

Trace gas emissions determined by this IDM method have previously been compared with an inhouse tracer ratio method at this dairy housing site and have been discussed in Bühler et al. (2021). Means from both methods were within the uncertainty range of the tracer method (<10%).

2.4 Deposition modelling

The bLS model modified by (Häni et al. 2018) (R package *bLSmodelR* available at https://www.agrammon.ch/documents-to-download/blsmodelr/) was used to calculate dry deposition by multiplying the measured concentration increase with a proportionality constant called the deposition velocity (Wesely and Hicks 2000). The deposition velocity was approximated by a resistances approach (Sutton et al. 1995b), whereby the velocity is the inverse of the sum of several resistances to deposition that must be overcome. These include the aerodynamic, boundary layer and canopy resistances across the surface-atmosphere interface, which vary with micrometeorological, canopy and surface properties of the ecosystem. The first two resistances are calculated, while the latter can be either laboriously derived from models or depends on parameterisations which can vary significantly at the canopy level where the exchange processes take place (Flechard et al. 2011). Instead, a more practical approach was applied, in which the average between the possible upper and lower boundaries was used to estimate deposition. For the maximum possible deposition velocity ($v_{d,max}$), the canopy resistance was set to 0, i.e., assuming that the surface acts as a perfect sink, while the effects of boundary layer and canopy resistances on deposition were not considered for the minimum case. This method allows a simple, yet reasonable approximation of the likely deposition and corrected emissions therefore represent an average of the possible lower and upper flux magnitudes. The deposition flux F_d was modelled following Flechard et al.; Häni et al. (2018) by

$$F_d = -v_d * C_{TD} \quad \text{(eq. 3)}$$

Where v_d is the deposition velocity and C_{TD} was the modelled concentration at the touchdown of a trajectory at the adsorbing surface. The aerodynamic resistance (R_a) usually included in the v_d calculation was omitted, since v_d was investigated for the layer between the modelled effective ground level i.e., z_0 plus the displacement height d and the adsorbing surface z_0' and was therefore implicitly accounted for in the bLS dispersion model. Since the canopy resistance R_c was set to 0 in the maximum deposition flux model, the deposition velocity v_d was calculated as

$$v_d = \frac{1}{R_b + R_c} \rightarrow v_{d,max} = \frac{1}{R_b} \quad \text{(eq. 4)}$$

The boundary layer resistance R_b was calculated from equation 5 in Flechard et al. (2010) using the input variables: friction velocity $u*$, canopy temperature, roughness length z_0, and ambient air pressure. Although wet deposition was not taken into account, there were only few periods of rainfall or fog with valid measurements, hence the underestimation of calculated emissions during such periods is likely small. Also, the deposition of particulate NH_4^+ was not investigated. The R package *bLSmodelR* was used for all of the modelling (Häni 2022).

In addition, based on the average conditions during the measurement campaign at the dairy housing, the fraction of the emission deposited within different distances (10, 20, 50, 100, 200 m) downwind of the source was modelled. From a simple mass balance perspective, the total horizontal flux through a vertical plane P_x at distance x which is perpendicular to the average wind direction (and sufficiently wide to capture the entire plume) will match the net flux, i.e., the sum of emissions Q_i and the integrated deposition flux $F_{d,\text{upw}} = \iint_{x<x_{\text{plane}}} F_d dxdy$, upwind of the plane:

$$\iint_{P_x} \overline{uc}\, dy\, dz = \sum_i Q_i + F_{d,\text{upw}} \quad \text{(eq. 5)}$$

Where $\overline{uc}$ is the temporal average of the product between the horizontal wind speed component along the main wind direction u and the concentration c.

If we solely focus on a single source (and its contribution to the horizontal flux) and divide equation eq. 5 by its source strength Q, we obtain the following relationship:

$$\iint_{P_x} \frac{\overline{uc}}{Q} dy\, dz = 1 + \frac{F_{d,\text{upw}}}{Q} \quad \text{(eq. 6)}$$

The ratio $F_{d,\text{upw}}/Q$ represents the ratio between the total deposition (related to the source emission) between source and plane P_x and the source emission strength. The ratio of the horizontal flux and the source strength is obtained from bLS model results as:

$$\frac{\overline{uc}}{Q} = \left(\frac{\overline{uc}}{E}\right)_{bLS} A_{source}^{-1} \quad \text{(eq. 7)}$$

With A_{source} being the area of the emitting source. Due to biases stemming from both the discretization and the stochastic nature of the bLS model, the integral of the horizontal flux from model results without accounting for deposition will never be exactly equal to 1. Thus, equation eq. 5 has been reformulated and discretised to provide:

$$\frac{F_{d,\text{upw}}}{Q} = A_{source}^{-1} \sum\sum \left(\left(\frac{\overline{uc}}{E}\right)_{bLS,dep} - \left(\frac{\overline{uc}}{E}\right)_{bLS}\right) \Delta y \Delta z \quad \text{(eq. 8)}$$

Where the subscripts bLS and bLS, dep stand for model results without deposition and with deposition, respectively. The plane's extensions were taken as 200 m in the crosswind direction and 80 m from model ground in the vertical direction. The discretization in the vertical was done in 20 steps on a logarithmic scale, where the discretization in the crosswind direction was equally spaced with 1 m distances.

2.5 Uncertainty analysis

The uncertainty analysis followed Bühler et al. (2021), whereby the uncertainty ε_Q of the mean IDM emission rate $\bar{Q}_i$ over a time period Δt was estimated from the standard deviation *SD* of consecutive measurements of increasing lengths from 1 h to 45 h using the longer first measurement period at the dairy housing (eq. 9) and represents the upper uncertainty boundary of the mean emission rates across the entire campaign.

$$\varepsilon_Q(\Delta t) = 2 * SD\{\bar{Q}_i(\Delta t)\} \quad \text{(eq. 9)}$$

Since the *SD* included true variations of *Q*, such as diel variability, the uncertainty, $\varepsilon_Q(\Delta t)$, corresponds to a 95% confidence interval of an assumed constant *Q* over time and is thus larger than the true uncertainty of the varying *Q*.

2.6 Data processing and assessment

For the IDM measurements, the 3D wind vectors (*u, v, w*) underwent two-axis coordinate rotations, corrections for a known bug affecting the *w* wind component of the Gill Windmaster instruments (Gill Instruments 2016), and were averaged to 30 min intervals. To correct for possible underestimation of NH_3 concentrations from loss by dry deposition the maximum dry deposition was modelled (Section 2.4), which represented an upper total emission boundary compared to the uncorrected emissions, which represented the lower boundary.

The bLS model cannot deal with periods of low wind speed, very high stability or instability, as well as extreme turbulence which are typically filtered out (Gao et al. 2009; Harper et al. 2010; Flesch et al. 2014). However, to avoid substantial data loss due to the meteorological conditions, a custom filtering procedure was applied based on observed variations of *u* and *v*, as well as literature values as described in Bühler et al. (2021). The filters at the dairy housing and the WWTP included friction velocity $u*$ >0.1 m s^{-1} or >0.05 m s^{-1} and for canopy height (z_H) and roughness length z_0, z_H /100 < z_0 <

$z_H/3$ or z_0 <0.1, respectively, while the ratio of the *SD* of the along-wind (σ_u) or crosswind speeds (σ_v) to $u*$, i.e., $\sigma_u/u*$ and $\sigma_v/u*$ were <4.5 at the dairy housing and <6 at the WWTP, and at both sites $|L|$ >2 m for the Obukhov length and the Kolmogorov constant of the Lagrangian structure function was 3 <*C0* <10. Finally, only wind directions perpendicular to the instrument paths and therefore including the plume were retained (e.g., SW at the WWTP or SW and NE at the dairy housing). This resulted in 282 and 379 valid half-hourly measurements corresponding to a data loss of 80% and 62% during autumn and winter, respectively, at the dairy housing and 241 intervals at the WWTP corresponding to an average of 69% data loss. Since data loss occurred mostly at night, daytime data retention was as high as 40 to 60% (Figure SI1.2). There was a general bias towards more daytime data and greater loss at dawn and dusk due to the rapid changes in atmospheric turbulence conditions and the higher frequency of fog which obscures the sensors during these periods. The iTRM included 290 valid datapoints with corresponding 30-min IDM means for the comparison split across the autumn (190 intervals) and winter (100 intervals) measurements.

Welch t-tests and Pearson correlations were used to compare means and establish synchronous correlations with predictor variables, while a cross correlation function was used to investigate lagged correlations.

The WWTP consisted of several structures that acted as sources with different emission strengths within the general source area, therefore a source weighting factor based on literature values from Samuelsson et al. (2018) for a WWTP and Kupper et al. (2020) for pig slurry tanks representing the sludge storage emission was applied to each source (see Bühler et al. 2022). Each area A_i with an emission E_i was combined to a single source with mean D_{avg}

$$D_{avg} = \sum_{i=1}^{N} E_i * w_i \quad \text{(eq. 10)}$$

using a weighting w_i calculated as follows

$$w_i = \frac{\sum_{j=1}^{N} A_j}{\sum_{j=1}^{N} (E_j/E_i * A_j)} \quad \text{(eq. 11)}$$

Other R packages used for data processing and plotting included *ibts* (Häni, 2022), *RgoogleMaps* (Loecher and Ropkins, 2015), *scales* (Wickham and Seidel. 2020), *ggplot2* (Wickham, 2016), *dplyr* (Wickham et al., 2022), *leaflet* (Cheng et al., 2022) and *openair* (Carslaw and Ropkins, 2012).

Results

3.1 Dairy housing

The meteorological conditions were generally representative for the respective seasons with mean ± standard deviation (*SD)* temperatures of 11.2 ± 4.6 °C and 3.6 ± 4.1 °C and mean monthly precipitation of 46 mm and 97 mm, respectively, for the autumn and winter periods at the dairy housing. Air temperatures were in the upper ranges during the autumn period and there were multiple events with high wind speeds particularly during winter at the dairy housing (Figure SI1.1 and SI1.3).

3.1.1 NH_3 emissions and diel profiles

The mean (±*SD*) NH_3 emissions during the autumn and winter measurement periods are shown in Table 1 for both emissions without accounting for dry deposition, which indicated the lower emission range, and with corrections for maximum dry deposition representing the upper range. The averages of these ranges present a mean estimate of the actual emissions resulting in 1.57 ± 0.59 kg NH_3 d^{-1} and 0.81 ± 0.38 kg NH_3 d^{-1} during autumn and winter, respectively. Correcting for dry deposition raised the uncorrected emissions by approx. 22% and the overall uncertainty of the IDM was 27%. This resulted in mean (± *SD*) corrections of the emissions to account for deposition of 0.28 ± 0.10 and 0.15 ± 0.07 kg NH_3 d^{-1} for the autumn and winter periods, respectively, with mean modelled deposition velocities of 1.1 ± 0.52 cm s^{-1} and 1.4 ± 0.55 cm s^{-1}. The measurement timeseries (Figure 3) presents the emissions accounting for mean deposition loss. Mean (±*SD*) NH_3 concentrations as measured by the miniDOAS for the entire measurement duration were 10.65 ± 6.86 µg NH_3 m^{-3} and 19.19 ± 14.23 µg NH_3 m^{-3} for up- and downwind instruments, respectively (Figure SI1.4).

Profiles indicated a median diurnal pattern of NH_3 emissions with mean deposition corrections from the dairy housing with peak emissions during the afternoon which were more pronounced in autumn compared to winter (Figure 4). Emissions correlated best with air temperature (r = 0.51, p <0.001), which slightly increased with a lag of 1-2 h for both periods and wind directions (up to r = 0.55, see Table SI1.1). Due to the relatively larger loss of data during the night, only the daytime emission profiles were considered robust.

3.1.2 Wind sector differences

Winds were predominantly from the NE and the SW during the autumn and winter measurement periods, respectively (Figure SI1.5).

Winds speeds were only higher from the SW during the winter with 3.9 ± 1.4 m s^{-1} compared to 1.9 ± 0.6 m s^{-1} from the NE while speeds were approx. 2.1 ± 0.8 m s^{-1} from both directions in autumn (Figure 5). Although wind speeds were different only in winter, emissions in autumn were 20% higher with NE winds over SW winds (Figure SI1.6a). During this period, emissions additionally correlated with u^* with NE but not the SW winds (Figure SI1.6b).

3.1.3 Comparisons with iTRM

Daily averaged NH_3 emissions from the dairy housing quantified by iTRM (mean ± *SD*) were 1.90 ± 0.58 kg NH_3 d^{-1} and 1.00 ± 0.31 kg NH_3 d^{-1} for autumn and winter measurements, respectively, for which only concurrent 30-min measurement intervals were used, hence these IDM means differed from those reported in table 1. Therefore, mean corrected emissions by IDM for these respective periods were 1.53 ± 0.59 kg NH_3 d^{-1} and 0.83 ± 0.34 kg NH_3 d^{-1}, varying up to 20% which was a statistically significant difference determined by Welch's T-test (*t-statistic* = 5.73, p <0.001).

3.1.4 Modelled deposition loss with distance from the source

The fraction of mean deposition to emission with distance from the source based on the measurement setup at the dairy housing was highest for stable atmospheric conditions and lowest for unstable conditions (Figure 6). For each respective condition the highest relative deposition within the first 50 – 150 m from the source, as relevant at our sites, ranged from 9 to 12% and 7 to 9%, respectively.

3.2 WWTP

The meteorological conditions during the measurements at the WWTP in 2019 were representative for the season with a mean ± *SD* temperature of 9.38 ± 2.58 °C and monthly precipitation of 126 mm, albeit with periods where temperatures were in the upper ranges or with high wind speeds (Figure SI2.1).

3.2.1 Mean NH_3 emissions

Average (mean ± *SD*) NH_3 emissions from the WWTP assuming no deposition loss (lower range) were 1.77 ± 0.84 kg NH_3 d^{-1}, while emissions corrected for maximum deposition (upper range) were 2.79 ± 1.28 kg NH_3 d^{-1}. Averaged emissions representing a mean corrected estimate of deposition were 2.27 ± 1.53 kg NH_3 d^{-1} (Figure 7), which resulted in a deposition correction of 28% with an overall uncertainty of IDM at 24%. The per person equivalent of the mean emissions corresponded to 18.4 g NH_3 PE^{-1} yr^{-1}, which represented 0.63% of the nitrogen (NH_4-N) inflow. The mean deposition correction for the emissions was 0.51 ± 0.23 kg NH_3 d^{-1} and the mean deposition velocity was 0.65 ± 0.40 cm s^{-1}. Mean (±*SD*) concentrations as measured by the miniDOAS instruments up- and downwind of the WWTP were 4.71 ± 0.82 µg NH_3 m^{-3} and 7.19 ± 1.55 µg NH_3 m^{-3}, respectively (Figure SI2.3).

3.2.2 Emission responses to management activities

Although a pH above 7 increases the partitioning of NH_3 to NH_4^+ and the temporal pattern of emissions was similar to that of pH (mean 7.4 ± 0.2) measured at the inflow (Figure 8), there was only a weak concurrent correlation (Pearson's r = 0.15, p <0.05). Using a cross correlation function to determine asynchronous leads and lags, statistically significant lagged relationships were found up to 5.5 h after changes in pH with peak correlations at 3 h (r = 0.52, F-statistic = 29.3, p <0.001). All sewage sludge tank agitators were operated on Monday mornings (06:00 – 12:00 local time on 30th September and 7th October), while one tank was additionally agitated more frequently during the week. However, no direct changes in emissions could be observed in response to agitation, as the two prominent agitation events coincided with measurement gaps.

As with the dairy housing, diurnal patterns in emissions were also evident and emissions peaked again around midday lagging behind management activities affecting pH or agitation times by 3-6 h, both of which peaked early morning (Figure 9). Emissions correlated moderately with air temperature (Pearson's $r = 0.48$, $p < 0.001$) which improved with a 3-hour offset ($r = 0.75$, $p < 0.001$), while incoming solar radiation also showed a high instantaneous correlation ($r = 0.67$, $p < 0.001$). A moderate correlation was also observed between emissions and wind speed ($r = 0.30$, $p < 0.001$).

Discussion

4.1 Dairy housing emissions

There were up to 20% differences in IDM-based emissions between main wind directions during the autumn measurements with higher emissions for NE compared to SW winds, although these were still within the uncertainty range estimated for IDM, i.e., <24% (Bühler et al. 2021). Increased emissions with NE winds, might have resulted from slightly higher wind speeds further indicated by the increased but still weak correlation of emissions with $u*$ for this direction only. However, in the winter period, wind speeds were even higher from the SW but did not result in differences in emissions. A more likely explanation was the diel shift in wind direction which was observed only in autumn reflecting daily emission patterns, whereby NE winds were more prevalent during the day and SW winds during the evening. However, we could not exclude the possibility that emissions may have been affected by different curtain settings, which were either half or fully open during autumn but fully closed in winter. Therefore, it is possible that the curtain settings affected the emission measurements, either from their position which increased aeration but also their presence affecting source geometry due to changes in turbulence conditions.

The diurnal pattern with higher daytime emissions, which was more prominent during the autumn measurement at the dairy housing, was probably mostly driven by air temperature (VanderZaag et al. 2015; Bougouin et al. 2016). Other studies found similar patterns for dairy housing emissions with daytime peaks being highest in summer, then transitional seasons and lowest in winter (Flesch et al. 2009; Saha et al. 2014). While wind speed showed no distinct diel patterns, it was higher during the winter period when emissions were lower further indicating the dominant effect of temperature compared to wind speed. This follows similar findings by Schrade et al. (2012), in which total emissions across six farms measured with iTRM showed a correlation with wind speed but the effects of air temperature and milk urea content were more dominant. This has also been observed for different housing types and manure management systems (Saha et al. 2014; Bougouin et al. 2016).

The comparison of NH_3 emission estimates between IDM and iTRM showed good agreement with an overall deviation of <20%, i.e., within the uncertainty of IDM. The possible underestimation by IDM with an averaged deposition correction may indicate that the correction was too low. In fact, the estimates with corrections for maximum deposition more closely matched emissions determined by iTRM (<3% difference). Although instrument precision and dispersion modelling may contribute to this difference, our results indicate that deposition is likely the main contributor. This conclusion agrees with results from Bühler et al. (2021) who observed smaller differences between IDM and iTRM of <10% for methane emissions, for which deposition is not relevant. Even though the slurry tank contributions were minor since it was covered, it is worth noting that iTRM did not include these emissions.

In general, our measurements were within typical ranges from the literature for loose housings with solid floors and no exercise yard during only transition seasons (spring and autumn) and winter, which ranged from 3.5 to 92.9 g NH_3 LU^{-1} d^{-1} and 5.2-87.9 g NH_3 LU^{-1} d^{-1} , respectively (Poteko et al. 2019). Compared to ranges published by Schrade et al. (2012) in Switzerland, the IDM measurements agreed well for the respective seasons, i.e., 28.0 ± 10.5 in autumn and 14.7 ± 6.9 g NH_3 LU^{-1} d^{-1} in winter compared with 16 - 44 g NH_3 LU^{-1} d^{-1} and 6 - 23 g NH_3 LU^{-1} d^{-1}, respectively. Other seasonal means for naturally ventilated barns with solid floors from a meta-analysis by Bougouin et al. (2016), which included different measurement methods, were comparable with autumn and winter averages around 31.6 ± 4.3 and 43.5 ± 29.9 g NH_3 cow^{-1} d^{-1}, respectively, compared to 39.2 ± 14.7 g NH_3 cow^{-1} d^{-1} and 20.2 ± 9.5 g NH_3 cow^{-1} d^{-1} (note the different units, as LU was not available). The winter mean is biased high due to higher emissions from two studies in the UK and USA. Including all seasons, mean annual emissions were 47.7 g NH_3 cow^{-1} d^{-1}, therefore the autumn and winter means were a factor of 0.66 and 0.91 of the annual mean, respectively, while the seasonal weighting factors derived from means in Schrade et al. (2012) were 0.96 and 0.49, respectively. The factors of seasonal to annual mean emissions were closer to those from Schrade et al. (2012), in which winter emissions were a factor of 0.6-0.8 lower than the autumn ones, while the values in this study were 0.53 of those in autumn. Saha et al. (2014) measured seasonal averages for winter and autumn ranging between 7.9-35.3 and 5.5-54.7 g NH_3 LU^{-1} d^{-1} for naturally ventilated housings using the carbon dioxide balance method. Their seasonal average weightings were 0.54 and 0.75 for winter and autumn, respectively, compared to the annual mean and the mean ratio of winter to autumn, i.e., 0.71, were similar to those listed above. Although comparing very well to other studies, it is likely that our daily means were slightly biased high due to the lower representation of transitional (dawn and dusk) and nighttime periods because atmospheric conditions during these times deviated from the assumed ideal conditions for IDM leading to data rejection. In addition to the daily data representativeness, it is important to consider the seasonal impacts when comparing emission measurements and applying annual emission factors.

Specifically compared to other line-integrated measurements from Flesch et al. (2009) who used a bLS model and measured whole farm, as well as separate source structures by relocating the sensors, of free-stall barns also equipped with semi-drawn curtains ,our measurements were in similar seasonal ranges and ratios, as their barn only emissions amounted to 21.2 ± 10.7 g NH_3 animal^{-1} d^{-1} in autumn and 11.7 ± 10.2 g NH_3 animal^{-1} d^{-1} in winter. They also found a similar but still weak diurnal patterns for the barns modulated only somewhat by air temperature in autumn and winter with $u*$ being of minor importance. Moreover, they found that the management practices across the different farms were the most influential on emissions (i.e., naturally ventilated free-stall barns, sand bedding, regularly scraped barn floors) and that the same IDM technique allowed good comparisons between locations.

4.2 WWTP emissions

Total emissions at the WWTP were higher than at the dairy housing and although fewer data were available, there was a much more prominent diurnal profile. Higher emissions are expected during the day due to higher N loads in the wastewater from human activity, but also from the higher temperatures driving emissions through increased molecular diffusion of NH_3 which enhances emissions from both the sludge and water line. However, peak air temperatures were often reached in the late afternoon while emissions peaked around noon leading to the higher offset correlation. Incoming solar radiation peaked at noon and showed a high synchronous correlation with emissions. Since many of the emission sources at the WWTP had open surfaces that were exposed to the sun (especially the sludge storage tanks, but also much of the water line), localised surface heating likely facilitated this higher correlation compared to ambient air temperature. With emissions being affected by weather conditions, as with the dairy housing, it is important to consider the impact of seasonality and representativeness of the measurement period for future comparisons. The emission profile also matched changes in pH and tank agitation following a time offset of 3-5.5 hours. Although NH_3 emissions are controlled by pH which determines the speciation of volatile NH_3 and non-volatile NH_4^+ with even microsite variations leading to observable emission changes (Hafner et al. 2013; Kim and Or 2019), the pH was measured at the inflow of the water line, which is expected to contribute only 34% to total emissions (Samuelsson et al. 2018), as opposed to the storage tanks by which point the pH will have changed. More likely, agitation of the open sludge tanks caused larger contributions to the total emission variations, as they are expected to produce the most emissions (Samuelsson et al. 2018), assuming they act as an open slurry tank (Kupper et al. 2020). However, agitation did not occur daily and regrettably, no direct effects of the agitation could be observed on emissions due to gaps in the measurements directly following the larger agitation events. Following the immediate initial emission response after disturbance in a swine slurry storage tank, Blanes-Vidal et al. (2012) observed a 1.5-3.5 h delay with a subsequent NH_3 emission increase without additional disturbance. This was explained by the development of a pH gradient during the transient-state conditions after disturbance and lasted up to 48 h. Therefore, the morning agitation of the sludge most likely promoted movement to and subsequent release of NH_3 at the surface and other buffers changing the pH profile and hence contributed to emission increases with delayed and lasting effects (Kupper et al. 2021). Longer measurement periods would be required to collect sufficient data and events to definitively determine the impact on emissions, as well as more expansive monitoring of facility parameters.

The NH_3 emissions of the WWTP (94.9 ± 44.1 g NH_3 h^{-1}) were smaller than measurements by Samuelsson et al. (2018) who reported 400 ± 100 g NH_3 h^{-1} for a much larger WWTP (805000 PE) in Gothenburg and using individual samplings at each processing stage during the day. When normalised by PE our measurements were over 4 times higher, i.e., 18.4 g NH_3 PE^{-1} yr^{-1} compared to 4.3 g NH_3 PE^{-1} yr^{-1} at the WWTP in Gothenburg. However, that plant included an activated sludge system comprised of nitrifying trickling filters and moving bed biofilm reactors for post-denitrification, which can be effective in lowering total NH_3 levels (Colón et al. 2009; Xue et al. 2010). The sludge after digestion was also dewatered with a centrifuge without intermediate liquid storage (personal communication S. Tumlin, Gryaab AB, Gothenburg). The solids were then stored for three weeks in open-air stockpiles before being transported off-site. Data from Aguirre-Villegas et al. (2019) on anaerobically digested dairy manure with and without solid-liquid separation using a screw press or centrifuge suggested that NH_3 emissions from the solid fraction can be lower by at least one order of magnitude compared to unseparated manure. If these findings are extrapolated to our WWTP to compare anaerobically digested liquid sewage sludge in open stores (i.e., without solid-liquid separation) with the storage of dewatered sludge in the Gothenburg plant, the discrepancy in PE normalised emissions seems plausible. Furthermore, our results come closer to the estimate by Sutton et al. (1995a) of 27 g NH_3 yr^{-1} for a WWTP in the UK.

Due to the lack of emission data from WWTPs, another comparison may be drawn with emissions from slurry stores. The matrix of sewage sludge is comparable to that of pig slurry, although it contains less NH_4^+ and the formation of a natural surface crust is less pronounced, which is expected to enhance emissions (Kupper et al. 2020). However, sewage sludge stores are agitated more frequently than slurry tanks (Kupper et al. 2015), likely enhancing NH_3 emissions. Emissions from slurry stores with different types of slurry and tank configurations are well documented (Kupper et al. 2020), allowing an estimation of the sewage sludge tank emissions based on pig slurry emission factors for comparable stores (i.e., 0.17 g NH_3 m^{-2} h^{-1}). Upscaled to the same source area as the WWTP, these emissions would amount to 80 g NH_3 h^{-1} which compare well with the measured emissions of 95 ± 64 g NH_3 h^{-1}, further confirming that the majority of measured emissions likely originated from the sludge storage.

4.3 Dry deposition corrections

Maximum dry deposition was modelled at both sites and the range averages between the maximum and no deposition resulted in emission corrections of 22-28% with higher percentages at the WWTP which had higher emissions. At the dairy housing, the correction differed with wind direction by 19% for NE winds but 27% and 23% for SW winds in autumn and winter, respectively. Although emissions were lower from the SW, atmospheric conditions were mostly stable which extended the footprint and allowed for a greater proportion of the emissions to be deposited. Since the relative correction with SW winds was greater in autumn than winter, it may be feasible that the curtain position, which was more frequently open during autumn, could have affected emission estimates by altering the turbulence conditions and hence possibly also the deposition corrections. Alternatively, the lower correction of 19% during both periods with NE winds may have resulted from the shorter measurement distance for NE emissions reducing the cumulative deposition loss. Overall, the absolute corrections were lower during winter even with higher wind speeds since temperatures and hence emissions were also low.

While both the heights of the emission source and measurements can affect the proportion deposited with distance, the bLS model assumes an emission at surface level, while the measurement heights and distances from the emission source varied between 1.2-1.7 m and 60-150 m, respectively, depending on site and direction. To estimate the relative deposition loss with distance, we modelled the fraction of deposition to emission for each stability condition for the dairy housing site. For the measurement distance of 150 m, the model indicated that at most 12% of the emissions were deposited during stable and less than 9% during unstable conditions, while minimal deposition at 50 m ranged from 7-9%. This proportion is in contrast to the emission correction value discussed previously, which adjusted the concentration loss detected at the measurement point with the associated footprint that changes the contribution weightings of both source and deposition areas.

Mean deposition velocities (i.e., the inverse of the sum of all resistances where canopy resistance was 0) at both sites were comparable to or lower than estimates from other studies (Phillips et al. 2004; Schrader and Brümmer 2014; McGinn et al. 2016), i.e., 0.65-1.55 cm s^{-1} and therefore the sum of boundary layer and canopy resistances were 0.64-1.54 s cm^{-1}. The model produced highest velocities at the dairy housing with SW winds during winter when emissions were lower, but wind speeds were higher, also evident from higher correlations with $u*$. In contrast, Phillips et al. (2004) found higher daytime v_{dep} in summer than winter of 3.94 ± 2.79 cm s^{-1} and 2.41 ± 1.92 cm s^{-1}, respectively, when emissions were higher even though wind speeds were lower than in winter. The surfaces between the source and measurement paths at both sites consisted of pastures and fallow fields which led to low roughness lengths z_0 of 0.01-0.03 ± 0.01 m. The higher value of 0.03 ± 0.01 m was only during NE winds at the dairy housing, which traversed a taller pasture.

Although most studies rely on simple resistance-based deposition models (Nemitz et al. 2000) and only few use bi-directional models with a calculated compensation point (Massad et al. 2010), the emission component downwind of a plume will be negligible for calculating the deposition loss relative to the total emission of a source. However, direct measurements of net NH_3 fluxes within the downwind plume would allow a better comparison but to date only very few data of net flux measurements are available (Swart et al. 2023 and references therein). Overall, the relative deposition values at the given measurement distances, surface roughness, stability conditions, and source heights were close to the ranges from studies including results of bi-directional models (Loubet et al. 2006; Asman et al. 1998). For comparable conditions, Asman et al. (1998) estimated a dry deposition loss within 100 m of 10% with greater amounts expected over rough surfaces with more turbulence due to higher deposition velocities. Using a N deposition model Schou et al. (2006) calculated cumulative losses from a dairy farm resulting in only 5% deposition within 100 m, 10% in 300 m, and 12% by 500 m, while Fowler et al. (1998) estimated 3-10% deposition within 300 m from a poultry farm based on a transect of concentration measurements from which the canopy resistance for the deposition model was determined by a regression fit. Estimates of dry deposition using resistance and dispersion models based on emission measurements from a hog farm in North Carolina (barns with forced ventilation and a slurry lagoon) were found to be even lower, i.e., 2.9-7% within 500 m and added up to only 16.6% with a distance of 2500 m (Bajwa et al. 2008). Although pig slurries can produce slightly higher NH_3 emissions from lagoons (Kupper et al. 2020), their deposition velocities were an order of magnitude lower than observed here, which the authors explained by the tendency of the deposition model used to underpredict under the given field conditions. Another study at a pig farm in South China estimated monthly means of 4.1-14% NH_3 deposition at 500 m applying passive samplers and a multi-resistance model (Yi et al. 2021). A multiapproach study downwind of a beef feedlot in North Carolina also found relative deposition amounts of approx. 14% at 500 m using resistance modelling and flux gradient measurements (McGinn et al. 2016), while Staebler et al. (2009) found dry deposition to account for 6-12% loss within 1 km from a similarly large feedlot in Canada using airborne concentration measurements and a deposition model. Our modelled relative deposition loss compared well with these studies but highlighted the variability due to different surface properties and estimation methods of emissions, as well as models needed to derive deposition fluxes. Hence, there is a need to further constrain deposition estimates through improved models or direct measurements of deposition fluxes within emission plumes.

Conclusions

This study demonstrated the application of IDM accounting for deposition losses to determine total NH_3 emissions from large-scale structures, such as animal housings and WWTP, the latter of which were the first such measurements in Switzerland. The mean deposition-corrected NH_3 emissions were 1.19 ± 0.48 from a loose dairy housing and 2.27 ± 1.53 kg NH_3 d^{-1} for a WWTP which agreed with a direct comparison using an inhouse tracer ratio method at the dairy housing, as well as literature data where available. Clear diurnal patterns were observed, which were likely driven by air temperature and to a smaller degree also wind speed, but mostly by management practices with indications of lagged responses. Longer datasets spanning several months or more per season would be required to determine the contributions of the predictor variables variations and capture more representative management activities. This could be achieved with IDM's continuous measurement operations but can be biased towards daytime periods due to requirements of specific atmospheric and site conditions, such as consistent wind directions, atmospheric turbulence conditions, and horizontally homogenous surfaces.

Currently, the main limitation of IDM is the higher uncertainty introduced by the deposition corrections which can also limit the ability to link emissions to specific activities if the effects on emissions fall within the uncertainty.

The comparison with the tracer method indicated that our mean estimates for corrections may be underestimating deposition. Even though the modelled deposition to emission fractions with distance compared well to previous studies, more precise methods to determine dry deposition or further validation experiments of deposition models are needed to improve the usefulness of IDM, such as to assess potential emission reducing management activities and technologies. With improved deposition corrections and longer measurement durations, IDM provides an excellent tool to evaluate complex facility-scale NH_3 emissions.

Acknowledgements

Funding was obtained from the Swiss Federal Office for the Environment (Contract 00.5082.P2I R254-0652 for the dairy housing measurements and Contract 06.0091.PZ / R281-0748 for the WWTP). We thank Michael Zähner (Ruminant Nutrition and Emission Research Group, Agroscope, Tänikon), Kerstin Zeyer and Simon Wyss (Laboratory for Air Pollution/Environmental Technology, EMPA, Dübendorf) for conducting the iTRM measurements and the operators of the WWTP Moossee-Urtenenbach, specifically B. Oberer, as well as Wenzel Gruber and Tobias Bührer (Eawag) for their support. We are grateful to Markus Jocher (Climate and Agriculture Group, Agroscope, Zürich) for supporting the operation of the measurement devices. Support with modelling issues and interpretation of the data by Christof Ammann (Climate and Agriculture Group, Agroscope, Zürich) and Albrecht Neftel (NRE) is gratefully acknowledged. Finally, we thank the farmers, namely Walter Denzler, Wängi and those surrounding the WWTP for their collaboration and allowing the placement of the measurement devices.

1. Publication bibliography

Abegglen, Christian; Siegrist, Hansruedi (2012): Mikroverunreinigungen aus kommunalem Abwasser. Verfahren zur weitergehenden Elimination auf Kläranlagen. Federal Office for the Environment FOEN. Bern (Umwelt-Wissen Nr., 1214). Available online at https://www.bafu.admin.ch/bafu/de/home/themen/wasser/publikationen-studien/publikationen-wasser/mikroverunreinigungen-aus-kommunalem-abwasser.html, checked on 12/21/2021.

Aguirre-Villegas, Horacio A.; Larson, Rebecca A.; Sharara, Mahmoud A. (2019): Anaerobic digestion, solid-liquid separation, and drying of dairy manure: Measuring constituents and modeling emission. In *Sci. Total Environ.* 696, p. 134059. DOI: 10.1016/j.scitotenv.2019.134059.

Asman, W. A. H. (1998): Factors influencing local dry deposition of gases with special reference to ammonia. In *Atmos. Environ.* 32 (3), pp. 415–421.

Asman, W. A. H.; Sutton, M. A.; Schjørring, J. K. (1998): Ammonia: emission, atmospheric transport and deposition. In *New Phytol* 139 (1), pp. 27–48. DOI: 10.1046/j.1469-8137.1998.00180.x.

Asman, W. A. H.; van Jaarsveld, Hans A. (1992): A variable-resolution trapsort model applied for NHx in Europe. In *Atmos. Environ.* 26A (3), pp. 445–464.

Bajwa, K. S.; Arya, S. P.; Aneja, V. P. (2008): Modeling studies of ammonia dispersion and dry deposition at some hog farms in North Carolina. In *J. Air. Waste. Manag. Assoc.* 58 (9), pp. 1198–1207. DOI: 10.3155/1047-3289.58.9.1198.

Baldé, Hambaliou; VanderZaag, Andrew C.; Burtt, Stephen D.; Wagner-Riddle, Claudia; Evans, Leigh; Gordon, Robert et al. (2018): Ammonia emissions from liquid manure storages are affected by anaerobic digestion and solid-liquid separation. In *Agric. For. Meteorol.* 258, pp. 80–88. DOI: 10.1016/j.agrformet.2018.01.036.

Blanes-Vidal, V.; Guàrdia, M.; Dai, X. R.; Nadimi, E. S. (2012): Emissions of NH3, CO2 and H2S during swine wastewater management: Characterization of transient emissions after air-liquid interface disturbances. In *Atmospheric Environment* 54, pp. 408–418. DOI: 10.1016/j.atmosenv.2012.02.046.

Bougouin, Adeline; Leytem, April; Dijkstra, Jan; Dungan, Robert S.; Kebreab, Ermias (2016): Nutritional and Environmental Effects on Ammonia Emissions from Dairy Cattle Housing: A Meta-Analysis. In *Journal of environmental quality* 45 (4), pp. 1123–1132. DOI: 10.2134/jeq2015.07.0389.

Bühler, Marcel; Häni, Christoph; Ammann, Christof; Brönnimann, Stefan; Kupper, Thomas (2022): Using the inverse dispersion method to determine methane emissions from biogas plants and wastewater treatment plants with complex source configurations. In *Atmos. Environ.: X* 13, p. 100161. DOI: 10.1016/j.aeaoa.2022.100161.

Bühler, Marcel; Häni, Christoph; Ammann, Christof; Mohn, Joachim; Neftel, Albrecht; Schrade, Sabine et al. (2021): Assessment of the inverse dispersion method for the determination of methane emissions from a dairy housing. In *Agric. For. Meteorol.* 307, p. 108501. DOI: 10.1016/j.agrformet.2021.108501.

Calvet, S.; Gates, R. S.; Zhang, Guoqiang; Estelles, F.; Ogink, N. W. M.; Pedersen, S.; Berckmans, Daniel (2013): Measuring gas emissions from livestock buildings: A review on uncertainty analysis and error sources. In *Biosystems Engineering* 116 (3), pp. 221–231. Available online at https://www.sciencedirect.com/science/article/pii/S1537511012001936?via%3Dihub, checked on 1/25/2023.

Colón, Joan; Martínez-Blanco, Julia; Gabarrell, Xavier; Rieradevall, Joan; Font, Xavier; Artola, Adriana; Sánchez, Antoni (2009): Performance of an industrial biofilter from a composting plant in the removal of ammonia and VOCs after material replacement. In *J. Chem. Technol. Biotechnol.* 84 (8), pp. 1111–1117. DOI: 10.1002/jctb.2139.

Dai, Xiao-Rong; Saha, Chayan Kumer; Ni, Ji-Qin; Heber, Albert J.; Blanes-Vidal, Victoria; Dunn, James L. (2015): Characteristics of pollutant gas releases from swine, dairy, beef, and layer manure, and municipal wastewater. In *Water research* 76, pp. 110–119. DOI: 10.1016/j.watres.2015.02.050.

Federal Statistical Office (2020): Agriculture and food. Pocket statistics 2020. Edited by S. Meyre. Federal Statistical Office. Neuchâtel, Switzerland (Agriculture and forestry, 07).

Flechard, C.; Nemitz, E.; Smith, R. I.; Fowler, D.; Vermeulen, A. T.; Bleeker, A. et al. (2011): Dry deposition of reactive nitrogen to European ecosystems. A comparison of inferential models across the NitroEurope network. In *Atmos. Chem. Phys.* 11 (6), pp. 2703–2728. DOI: 10.5194/acp-11-2703-2011.

Flechard, C.; Spirig, C.; Neftel, A.; Ammann, C. (2010): The annual ammonia budget of fertilised cut grassland - Part 2: Seasonal variations and compensation point modeling. In *Biogeosciences* 7 (2), pp. 537–556. DOI: 10.5194/bg-7-537-2010.

Flesch, T. K.; Harper, L. A.; Powell, J. M.; Wilson, J. D. (2009): Inverse-dispersion calculation of ammonia emissions from Wisconsin dairy farms. In *Trans. ASABE* 52 (1), pp. 253–265. DOI: 10.13031/2013.25946.

Flesch, T. K.; McGinn, S. M.; Chen, D.; Wilson, J. D.; Desjardins, R. L. (2014): Data filtering for inverse dispersion emission calculations. In *Agric. For. Meteorol.* 198-199, pp. 1–6. DOI: 10.1016/j.agrformet.2014.07.010.

Flesch, T. K.; Vergé, X. P. C.; Desjardins, R. L.; Worth, D. (2013): Methane emissions from a swine manure tank in western Canada. In *Canadian Journal of Animal Science* 93 (1), pp. 159–169. DOI: 10.4141/cjas2012-072.

Flesch, T. K.; Wilson, J. D.; Harper, L. A.; Crenna, B. P. (2005): Estimating gas emissions from a farm with an inverse-dispersion technique. In *Atmos. Environ.* 39 (27), pp. 4863–4874. DOI: 10.1016/j.atmosenv.2005.04.032.

Flesch, T. K.; Wilson, J. D.; Harper, L. A.; Crenna, B. P.; Sharpe, R. R. (2004): Deducing ground-to-air emissions from observed trace gas concentrations: A field trial. In *J. Appl. Meteorol.* 43 (3), pp. 487–502. DOI: 10.1175/1520-0450(2004)043<0487:DGEFOT>2.0.CO;2.

Flesch, T. K.; Wilson, J. D.; Harper, L. A.; Todd, R. W.; Cole, N. A. (2007): Determining ammonia emissions from a cattle feedlot with an inverse dispersion technique. In *Agric. For. Meteorol.* 144 (1-2), pp. 139–155. DOI: 10.1016/j.agrformet.2007.02.006.

Fowler, D.; Pitcairn, C.E.R.; Sutton, M. A.; Flechard, C.; Loubet, B.; Coyle, M.; Munro, R. C. (1998): The mass budget of atmospheric ammonia in woodland within 1 km of livestock buildings. In *Environ. Pollut.* 102 (1), pp. 343–348. DOI: 10.1016/S0269-7491(98)80053-5.

Fowler, D.; Steadman, C. E.; Stevenson, D.; Coyle, M.; Rees, R. M.; Skiba, U. M. et al. (2015): Effects of global change during the 21st century on the nitrogen cycle. In *Atmos Chem Phys* 15 (24), pp. 13849–13893. DOI: 10.5194/acp-15-13849-2015.

Galloway, James N.; Bleeker, Albert; Erisman, Jan Willem (2021): The Human Creation and Use of Reactive Nitrogen: A Global and Regional Perspective. In *Annu. Rev. Environ. Resour.* 46 (1), pp. 255–288. DOI: 10.1146/annurev-environ-012420-045120.

Gao, Z.; Mauder, M.; Desjardins, R. L.; Flesch, T. K.; van Haarlem, R. P. (2009): Assessment of the backward Lagrangian Stochastic dispersion technique for continuous measurements of CH4 emissions. In *Agric. For. Meteorol.* 149 (9), pp. 1516–1523. DOI: 10.1016/j.agrformet.2009.04.004.

Gao, Zhiling; Desjardins, Raymond L.; Flesch, Thomas K. (2010): Assessment of the uncertainty of using an inverse-dispersion technique to measure methane emissions from animals in a barn and in a small pen. In *Atmos. Environ.* 44 (26), pp. 3128–3134. DOI: 10.1016/j.atmosenv.2010.05.032.

Gill Instruments (2016): Technical key note: Software bug affecting 'w' wind component of the WindMaster family. Gill Instruments. Lymington, UK. Available online at http://gillinstruments.com/data/manuals/KN1509_WindMaster_WBug_info.pdf.

Grant, Richard H.; Boehm, Matthew T.; Lawrence, Alfred F.; Heber, Albert J. (2013): Ammonia emissions from anaerobic treatment lagoons at sow and finishing farms in Oklahoma. In *Agric. For. Meteorol.* 180, pp. 203–210. DOI: 10.1016/j.agrformet.2013.06.006.

Hafner, S. D.; Montes, F.; Rotz, C. A. (2013): The role of carbon dioxide in emission of ammonia from manure. In *Atmos. Environ.* 66, pp. 63–71. DOI: 10.1016/j.atmosenv.2012.01.026.

Häni, C. (2021): bLSmodelR: bLSmodelR - An atmospheric dispersion model in R.

Häni, C.; Flechard, C.; Neftel, A.; Sintermann, J.; Kupper, T. (2018): Accounting for field-scale dry deposition in backward Lagrangian stochastic dispersion modelling of NH_3 emissions. In *Atmosphere* 9 (4), p. 146. DOI: 10.3390/atmos9040146.

Harper, L. A.; Denmead, O. T.; Flesch, T. K. (2011): Micrometeorological techniques for measurement of enteric greenhouse gas emissions. In *Anim. Feed Sci. Technol.* 166-167, pp. 227–239. DOI: 10.1016/j.anifeedsci.2011.04.013.

Harper, L. A.; Flesch, T. K.; Wilson, J. D. (2010): Ammonia emissions from broiler production in the San Joaquin Valley. In *Poultry Sci.* 89 (9), pp. 1802–1814. DOI: 10.3382/ps.2010-00718.

Hempel, Sabrina; Saha, Chayan Kumer; Fiedler, Merike; Berg, Werner; Hansen, Christiane; Amon, Barbara; Amon, Thomas (2016): Non-linear temperature dependency of ammonia and methane emissions from a naturally ventilated dairy barn. In *Biosyst. Eng.* 145, pp. 10–21. DOI: 10.1016/j.biosystemseng.2016.02.006.

Kafle, Gopi Krishna; Joo, HungSoo; Ndegwa, Pius M. (2018): Sampling Duration and Frequency for Determining Emission Rates from Naturally Ventilated Dairy Barns. In *Trans. ASABE* 61 (2), pp. 681–691. DOI: 10.13031/trans.12543.

Kim, Minsu; Or, Dani (2019): Microscale pH variations during drying of soils and desert biocrusts affect HONO and NH3 emissions. In *Nature communications* 10 (1), p. 3944. DOI: 10.1038/s41467-019-11956-6.

Kupper, T.; Bonjour, Cyrill; Menzi, H. (2015): Evolution of farm and manure management and their influence on ammonia emissions from agriculture in Switzerland between 1990 and 2010. In *Atmos. Environ.* 103, pp. 215–221. DOI: 10.1016/j.atmosenv.2014.12.024.

Kupper, Thomas; Bonjour, Cyrill; Achermann, B.; Rihm, B.; Zaucker, F.; Menzi, Harald (2013): Ammoniakemissionen in der Schweiz 1990-2010 und Prognose bis 2020. BAFU.

Kupper, Thomas; Eugster, Roy; Sintermann, Jörg; Häni, Christoph (2021): Ammonia emissions from an uncovered dairy slurry storage tank over two years: Interactions with tank operations and meteorological conditions. In *Biosyst. Eng.* 204, pp. 36–49. DOI: 10.1016/j.biosystemseng.2021.01.001.

Kupper, Thomas; Häni, Christoph; Neftel, Albrecht; Kincaid, Chris; Bühler, Marcel; Amon, Barbara; VanderZaag, Andrew (2020): Ammonia and greenhouse gas emissions from slurry storage - A review. In *Agric. Ecosyst. Environ.* 300, p. 106963. DOI: 10.1016/j.agee.2020.106963.

Loubet, B.; Asman, W. A. H.; Theobald, M. R.; Hertel, O.; Tang, Y. S.; Robin, P. et al. (2009): Ammonia Deposition Near Hot Spots: Processes, Models and Monitoring Methods. In M. A. Sutton, S. Reis, S. M. H. Baker (Eds.): Atmospheric Ammonia. Dordrecht: Springer Netherlands, pp. 205–267.

Loubet, B.; Cellier, P.; Milford, C.; Sutton, M. A. (2006): A coupled dispersion and exchange model for short-range dry deposition of atmospheric ammonia. In *Q. J. R. Meteorol. Soc.* 132 (618), pp. 1733–1763. DOI: 10.1256/qj.05.73.

Loubet, Benjamin; Carozzi, Marco; Voylokov, Polina; Cohan, Jean-Pierre; Trochard, Robert; Génermont, S. (2017): Evaluation of a new inference method for estimating ammonia volatilisation from multiple agronomic plots. In *Biogeosciences Discuss.*, pp. 1–32. DOI: 10.5194/bg-2017-424.

Massad, R.-S.; Nemitz, E.; Sutton, M. A. (2010): Review and parameterisation of bi-directional ammonia exchange between vegetation and the atmosphere. In *Atmos Chem Phys* 10 (21), pp. 10359–10386. DOI: 10.5194/acp-10-10359-2010.

McGinn, S. M.; Flesch, T. K.; Crenna, B. P.; Beauchemin, K. A.; Coates, T. (2007): Quantifying ammonia emissions from a cattle feedlot using a dispersion model. In *J. Environ. Qual.* 36 (6), pp. 1585–1590. DOI: 10.2134/jeq2007.0167.

McGinn, S. M.; Janzen, H. H.; Coates, T. W.; Beauchemin, K. A.; Flesch, T. K. (2016): Ammonia emission from a beef cattle feedlot and its local dry deposition and re-emission. In *J. Environ. Qual.* 45 (4), pp. 1178–1185. DOI: 10.2134/jeq2016.01.0009.

Mendes, Luciano B.; Edouard, Nadège; Ogink, Nico W.M.; van Dooren, Hendrik Jan C.; Tinôco, Ilda de Fátima F.; Mosquera, Julio (2015): Spatial variability of mixing ratios of ammonia and tracer gases in a naturally ventilated dairy cow barn. In *Biosyst. Eng.* 129, pp. 360–369. DOI: 10.1016/j.biosystemseng.2014.11.011.

Mohn, J.; Zeyer, K.; Keck, M.; Keller, M.; Zähner, M.; Poteko, J. et al. (2018): A dual tracer ratio method for comparative emission measurements in an experimental dairy housing. In *Atmos. Environ.* 179, pp. 12–22. DOI: 10.1016/j.atmosenv.2018.01.057.

Nemitz, Eiko; Sutton, Mark A.; Schjoerring, Jan K.; Husted, Søren; Paul Wyers, G. (2000): Resistance modelling of ammonia exchange over oilseed rape. In *Agric. For. Meteorol.* 105 (4), pp. 405–425. DOI: 10.1016/S0168-1923(00)00206-9.

Phillips, S. B.; Arya, S. P.; Aneja, V. P. (2004): Ammonia flux and dry deposition velocity from near-surface concentration gradient measurements over a grass surface in North Carolina. In *Atmos. Environ.* 38 (21), pp. 3469–3480. DOI: 10.1016/j.atmosenv.2004.02.054.

Poteko, Jernej; Zähner, Michael; Schrade, Sabine (2019): Effects of housing system, floor type and temperature on ammonia and methane emissions from dairy farming: A meta-analysis. In *Biosyst. Eng.* 182, pp. 16–28. DOI: 10.1016/j.biosystemseng.2019.03.012.

Poteko, Jernej; Zähner, Michael; Steiner, Beat; Schrade, Sabine (2018): Residual soiling mass after dung removal in dairy loose housings: Effect of scraping tool, floor type, dung removal frequency and season. In *Biosyst. Eng.* 170, pp. 117–129. DOI: 10.1016/j.biosystemseng.2018.04.006.

Saha, C. K.; Ammon, C.; Berg, W.; Fiedler, M.; Loebsin, C.; Sanftleben, P. et al. (2014): Seasonal and diel variations of ammonia and methane emissions from a naturally ventilated dairy building and the associated factors influencing emissions. In *Sci. Total Environ.* 468-469, pp. 53–62. DOI: 10.1016/j.scitotenv.2013.08.015.

Samuelsson, J.; Delre, A.; Tumlin, S.; Hadi, S.; Offerle, B.; Scheutz, C. (2018): Optical technologies applied alongside on-site and remote approaches for climate gas emission quantification at a wastewater treatment plant. In *Water Res.* 131, pp. 299–309. DOI: 10.1016/j.watres.2017.12.018.

Schou, Jesper S.; Tybirk, Knud; Løfstrøm, Per; Hertel, Ole (2006): Economic and environmental analysis of buffer zones as an instrument to reduce ammonia loads to nature areas. In *Land Use Policy* 23 (4), pp. 533–541. DOI: 10.1016/j.landusepol.2005.09.005.

Schrade, Sabine; Zeyer, Kerstin; Gygax, Lorenz; Emmenegger, Lukas; Hartung, Eberhard; Keck, Margret (2012): Ammonia emissions and emission factors of naturally ventilated dairy housing with solid floors and an outdoor exercise area in Switzerland. In *Atmos. Environ.* 47, pp. 183–194. DOI: 10.1016/j.atmosenv.2011.11.015.

Schrader, F.; Brümmer, C. (2014a): Land use specific ammonia deposition velocities: a review of recent studies (2004-2013). In *Water Air Soil Pollut.* 225 (10), p. 2114. DOI: 10.1007/s11270-014-2114-7.

Schrader, Frederik; Brümmer, Christian (2014b): Land Use Specific Ammonia Deposition Velocities: a Review of Recent Studies (2004-2013). In *Water Air Soil Pollut.* 225 (10), p. 2114. DOI: 10.1007/s11270-014-2114-7.

Sintermann, J.; Dietrich, K.; Häni, C.; Bell, M.; Jocher, M.; Neftel, A. (2016): A miniDOAS instrument optimised for ammonia field measurements. In *Atmos. Meas. Tech.* 9 (6), pp. 2721–2734. DOI: 10.5194/amt-9-2721-2016.

Sommer, S. G.; Christensen, M. L.; Schmidt, T.; Jensen, L. S. (2013): Animal Manure Recycling. Chichester, UK: John Wiley & Sons, Ltd.

Staebler, Ralf M.; McGinn, Sean M.; Crenna, Brian P.; Flesch, Thomas K.; Hayden, Katherine L.; Li, Shao-Meng (2009): Three-dimensional characterization of the ammonia plume from a beef cattle feedlot. In *Atmospheric Environment* 43 (38), pp. 6091–6099. DOI: 10.1016/j.atmosenv.2009.08.045.

Sutton, M. A.; Milford, C.; Dragosits, U.; Place, C. J.; Singles, R. J.; Smith, R. I. et al. (1998): Dispersion, deposition and impacts of atmospheric ammonia: quantifying local budgets and spatial variability. In : Nitrogen, the Confer-N-s: Elsevier, pp. 349–361.

Sutton, M. A.; Place, C. J.; Eager, M.; Fowler, D.; Smith, R. I. (1995a): Assessment of the Magnitude of Ammonia Emissions in the United Kingdom. In *Atmospheric Environment* 29 (12), pp. 1393–1411.

Sutton, M. A.; Schjorring, J. K.; Wyers, G. P.; Duyzer, J. H.; Ineson, P.; Powlson, D. S. (1995b): Plant-atmosphere exchange of ammonia [and discussion]. In *Philosophical Transactions of the Royal Society A: Mathematical, Physical and Engineering Sciences* 351 (1696), pp. 261–278. DOI: 10.1098/rsta.1995.0033.

Sutton, Mark A.; Oenema, Oene; Erisman, Jan Willem; Leip, Adrian; van Grinsven, Hans; Winiwarter, Wilfried (2011): Too much of a good thing. In *Nature* 472 (7342), pp. 159–161. DOI: 10.1038/472159a.

Swart, Daan; Zhang, Jun; van der Graaf, Shelley; Rutledge-Jonker, Susanna; Hensen, Arjan; Berkhout, Stijn et al. (2023): Field comparison of two novel open-path instruments that measure dry deposition and emission of ammonia using flux-gradient and eddy covariance methods. In *Atmos. Meas. Tech.* 16 (2), pp. 529–546. DOI: 10.5194/amt-16-529-2023.

van Damme, Martin; Clarisse, Lieven; Franco, Bruno; Sutton, Mark A.; Erisman, Jan Willem; Wichink Kruit, Roy et al. (2021): Global, regional and national trends of atmospheric ammonia derived from a decadal (2008–2018) satellite record. In *Environ. Res. Lett.* 16 (5), p. 55017. DOI: 10.1088/1748-9326/abd5e0.

VanderZaag, Andrew; Amon, Barbara; Bittman, Shabtai; Kuczyński, Tadeusz (2015): Ammonia Abatement with Manure Storage and Processing Techniques. In Stefan Reis, Clare Howard, Mark A. Sutton (Eds.): Costs of ammonia abatement and the climate co-benefits. Dordrecht: Springer, pp. 75–112.

Wesely, M.; Hicks, B. B. (2000): A review of the current status of knowledge on dry deposition. In *Atmos. Environ.* 34 (12-14), pp. 2261–2282. DOI: 10.1016/S1352-2310(99)00467-7.

Wu, Wentao; Zhang, Guoqiang; Kai, P. (2012): Ammonia and methane emissions from two naturally ventilated dairy cattle buildings and the influence of climatic factors on ammonia emissions. In *Atmos. Environ.* 61, pp. 232–243. DOI: 10.1016/j.atmosenv.2012.07.050.

Xue, Nian-tao; Wang, Qun-hui; Wu, Chuan-fu; Sun, Xiao-hong; Xie, Wei-min (2010): A pilot field-scale study on biotrickling filter treatment of NH3-containing odorous gases from organic waste composting plants. In *J. Zhejiang Univ. Sci. A* 11 (9), pp. 629–637. DOI: 10.1631/jzus.A1000095.

Yi, Wuying; Shen, Jianlin; Liu, Guoping; Wang, Juan; Yu, Lifei; Li, Yong et al. (2021): High NH 3 deposition in the environs of a commercial fattening pig farm in central south China. In *Environ. Res. Lett.* 16 (12), p. 125007. DOI: 10.1088/1748-9326/ac3603.

Figures

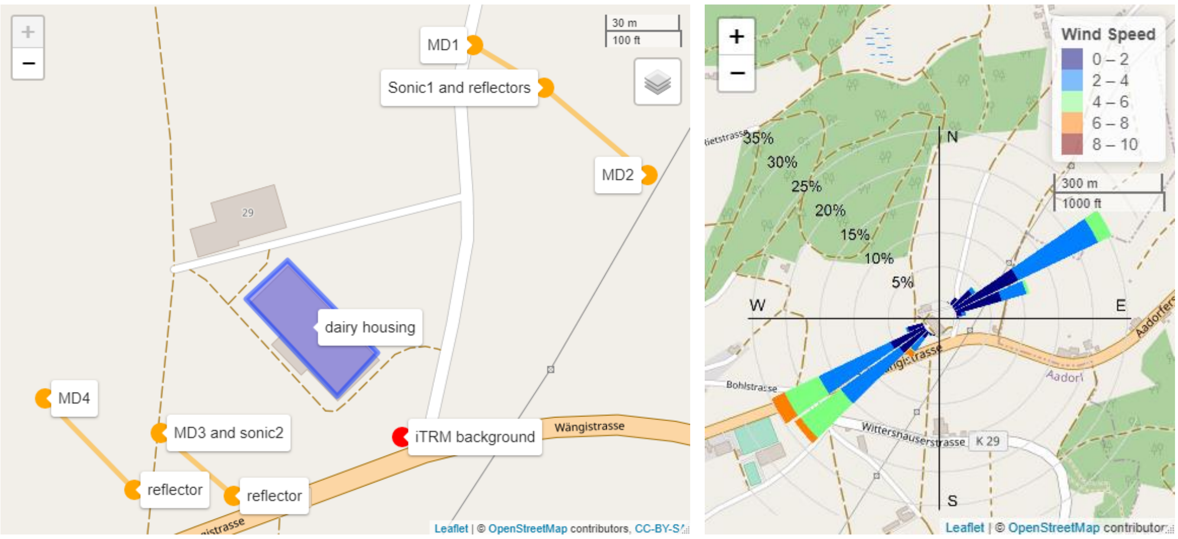

Figure 1. Map of the loose dairy housing (emitting area in blue) and instrument setup up and downwind of the housing (left) consisting of miniDOAS sensors and reflectors (MD1 to 4, orange dots and lines for measurement paths), sonic anemometers (sonic1 and 2), as well as the inlet for background concentration measurements needed for the iTRM (red dot). Wind speeds and frequencies during the entire measurement period (right) indicated two main directions. Map data ©OpenStreetMap contributors. Please see the online version for the full colours.

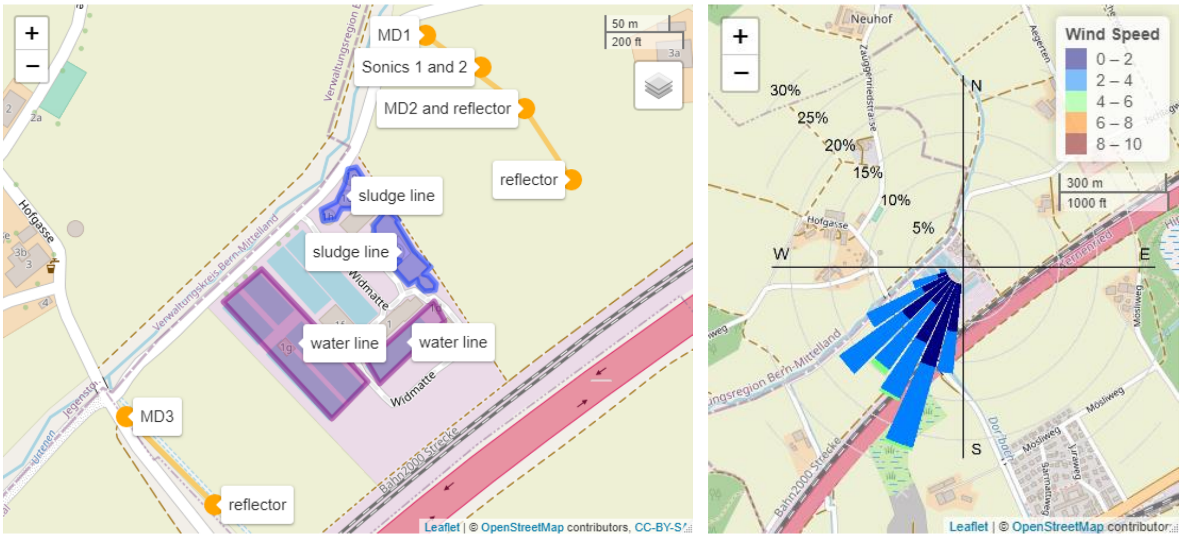

Figure 2. Map of the wastewater treatment plant with (left) emitting structures (blue shading for the sludge line and purple for the water line). Yellow dots and lines are the miniDOAS sensors and measurement paths (MD1 to 3) and sonic anemometers. Wind speeds and frequencies during the measurement period are shown on the right. Map data © OpenStreetMap contributors. Please see the online version for the full colours.

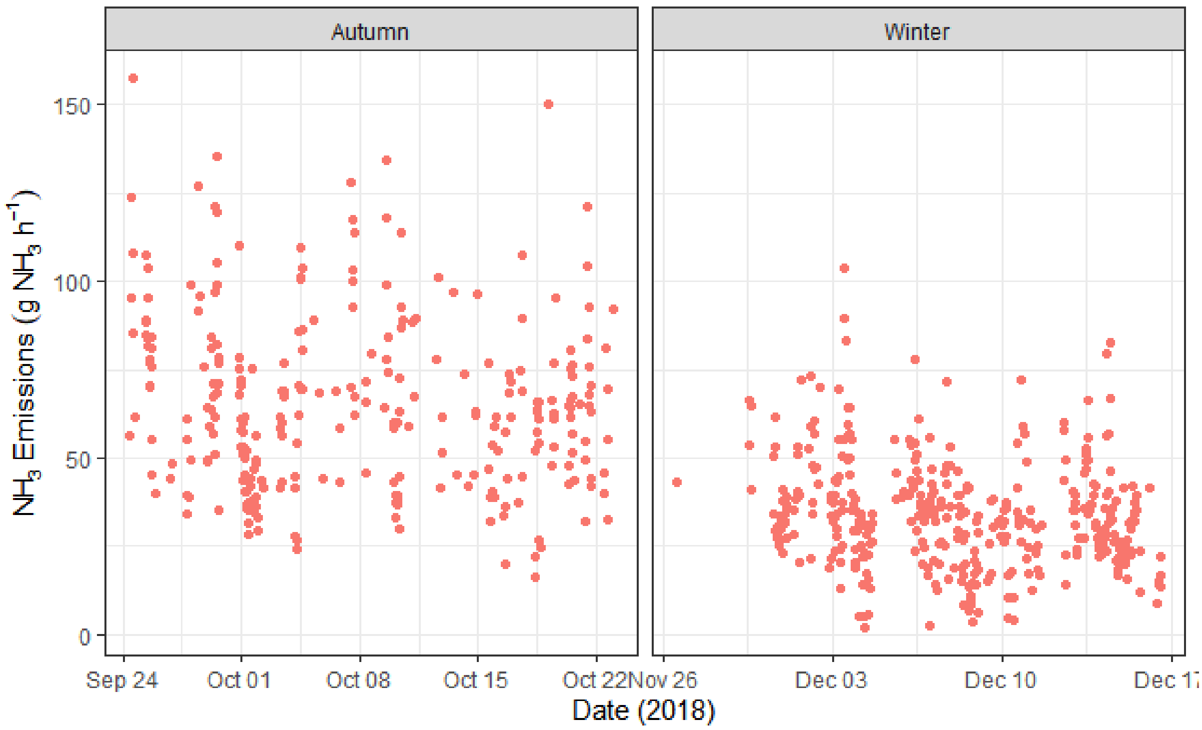

Figure 3. Timeseries of NH_3 emissions including averaged deposition loss for the first (left) and second (right) measurement periods at the dairy housing.

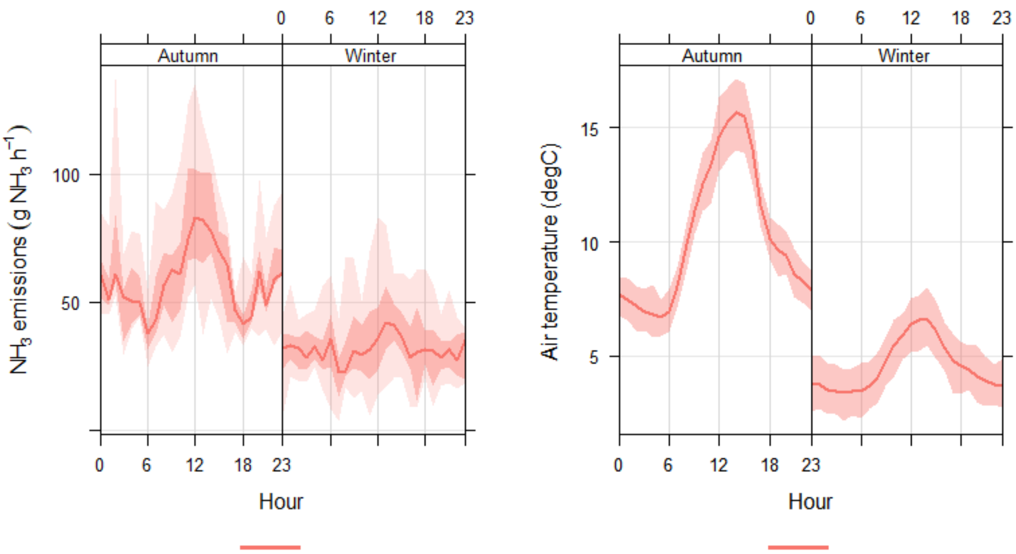

Figure 4. Diurnal patterns of median NH_3 emissions (left) including average deposition correction, as well as the mean air temperature profile (right) at the dairy housing for autumn and winter measurements, respectively.

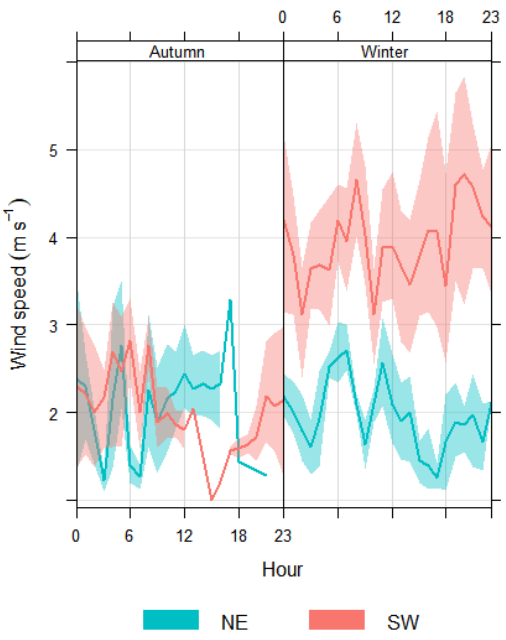

Figure 5. Mean diel profiles of wind speed separated by wind direction (northeast, NE, and southwest, SW) during both measurement periods.

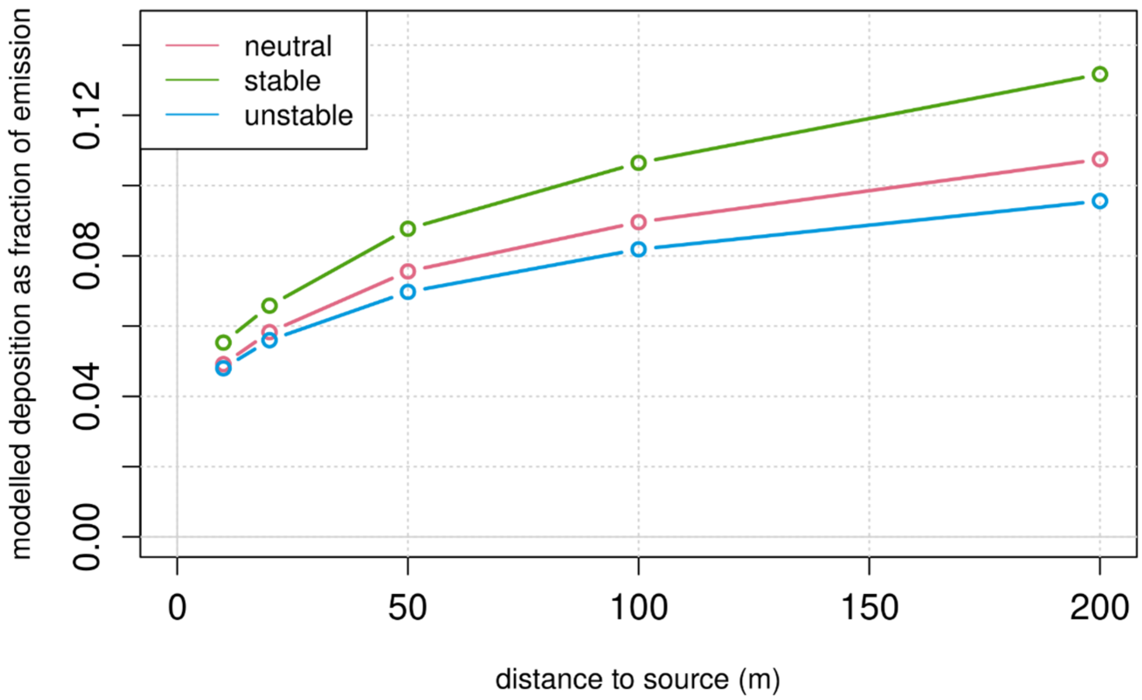

Figure 6. Relative NH_3 deposition as fraction of total emissions deposited with distance from the source depending on atmospheric stability conditions (defined as Obukhov length, L, -500< L <-50 for unstable, |L| >500 for neutral, and 10 < L <500 for stable).

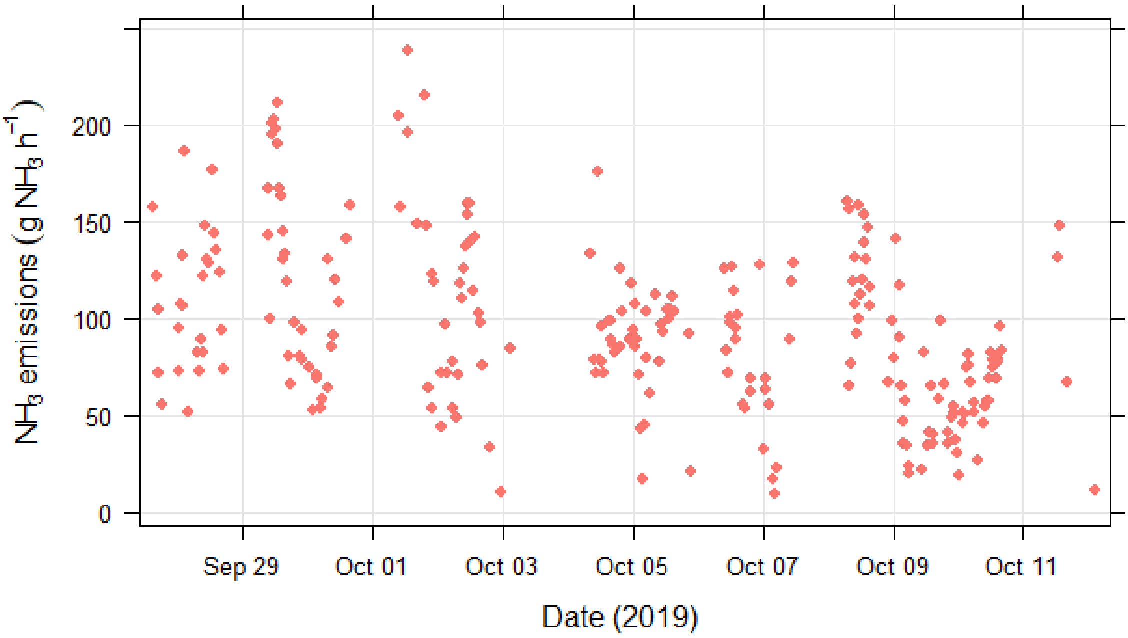

Figure 7. Timeseries of mean deposition-corrected NH_3 emissions filtered for ideal micrometeorological conditions.

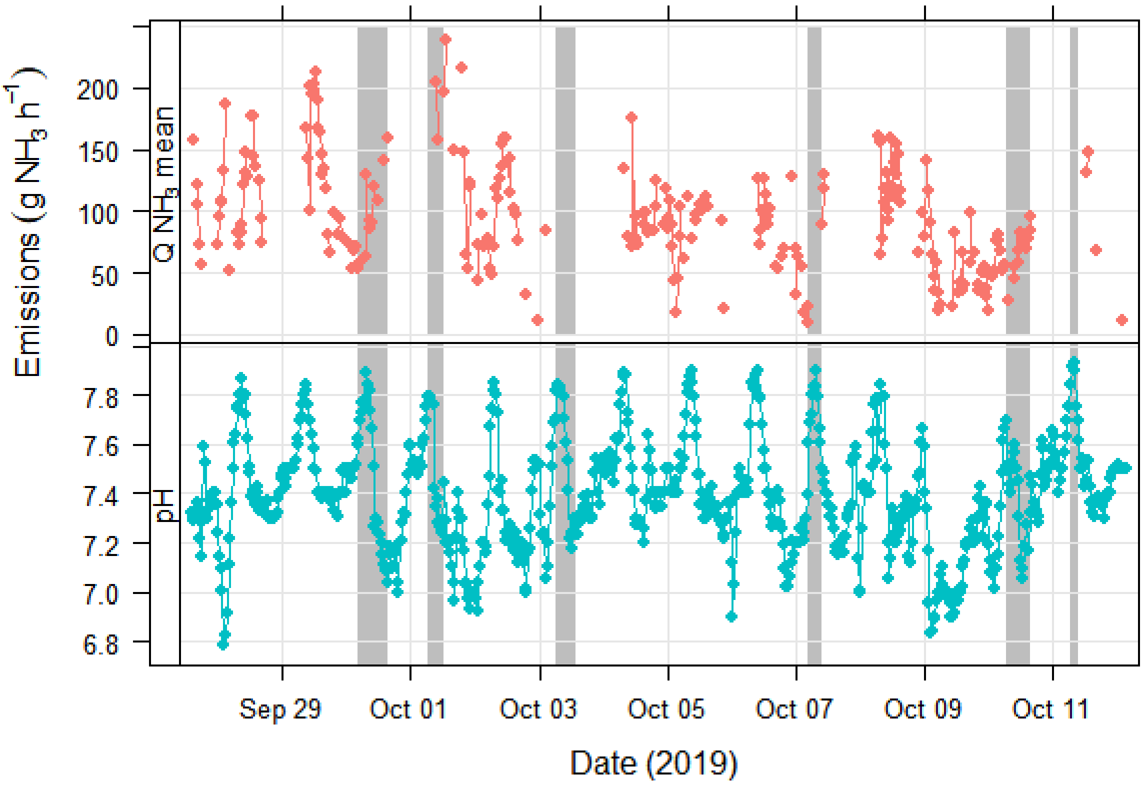

Figure 8. Timeseries of mean NH_3 emissions (top) and pH (bottom) at the inflow of the WWTP with agitation events (grey shaded bars) of the slurry storage tanks during the measurement period. Although

marked in grey over the pH changes, the agitation events did not have an effect on pH, as this was measured at the inflow to the water line and not at the sludge tanks.

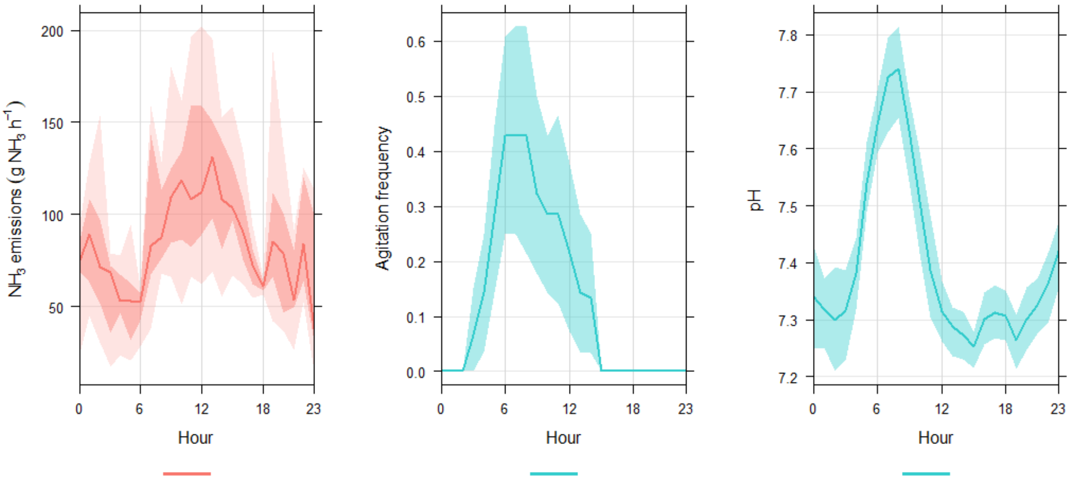

Figure 9. Diel profiles of median NH_3 emissions with deposition corrections (left), counts of agitation events mixing the sludge tanks (middle), and mean pH measured at the inflow (right).

Table 1. Mean and standard deviation (*SD*) of non-gap filled emissions for the whole dairy housing, as well as per livestock unit.

Duration	*Deposition correction*	*Mean ± SD NH_3 emissions*	
		(kg NH_3 d^{-1})	*(g NH_3 LU^{-1} d^{-1})**
Autumn	None	1.28 ± 0.5	22.8 ± 8.9
	Max	1.85 ± 0.69	33.0 ± 12.3
	Mean	1.57 ± 0.59	28.0 ± 10.5
Winter	None	0.66 ± 0.31	12.0 ± 5.6
	Max	0.97 ± 0.44	17.6 ± 8.0
	Mean	0.81 ± 0.38	14.7 ± 6.9
All	None	0.97 ± 0.40	17.6 ± 7.2
	Max	1.41 ± 0.56	25.6 ± 10.2
	Mean	1.19 ± 0.48	21.6 ± 8.7

* Livestock units (*LU* = 500 kg live weight)

Supplement: Ammonia emissions from dairy housing and a wastewater treatment plant quantified with an inverse dispersion method accounting for deposition loss

Alex C. Valach, Christoph Häni, Marcel Bühler, Joachim Mohn, Sabine Schrade, and Thomas Kupper

SI1. Dairy housing

SI1.1 Supplementary data

Additional figures on the weather conditions, site operations, data processing, and instrument outputs are presented below for both sites.

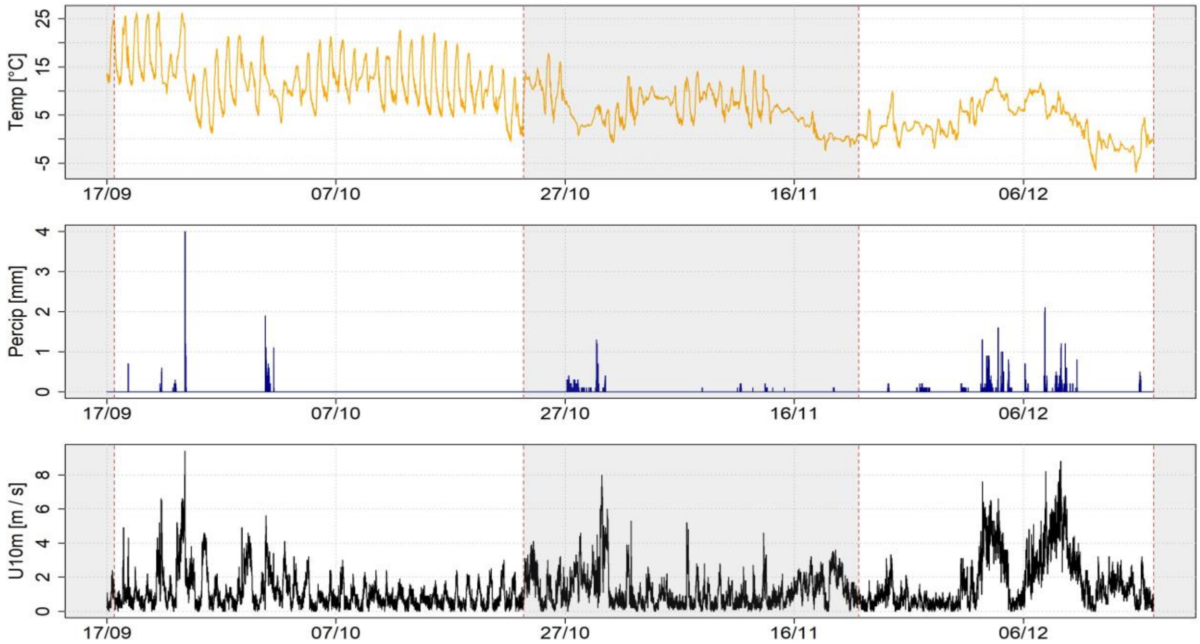

Figure SI1.1. Meteorological conditions (temperature, precipitation, and wind speed) from the nearby weather station (Taenikon in Aadorf, MeteoSwiss) during the first (autumn) and second (winter) measurement periods (non-shaded sectors) at the dairy housing in 2018. Reproduced from the supplemental information in Bühler et al. (2022).

Due to the filtering requirements (including valid wind directions, atmospheric turbulence and stability conditions, and bLS outputs) data retention was relatively low with a bias towards higher retention during the day than at night averaging in 69% data loss across all measurements (Figure SI1.2).

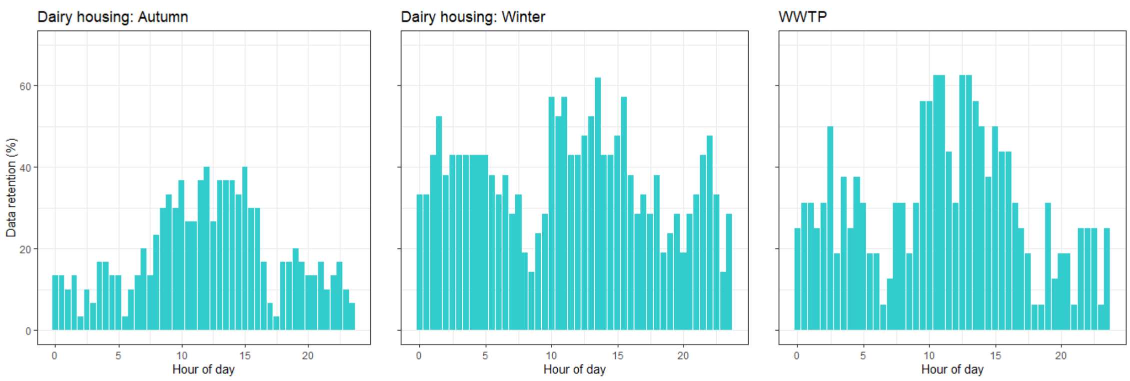

Figure SI1.2. Diel averages of data retention (as % of data available during instrument uptime) for both measurement periods at the dairy housing (left and middle panels) and the WWTP (right panel).

Since emissions could only be determined for wind directions perpendicular to the line-integrated measurements Figure SI1.3 indicates the dominant wind directions with time. In order to calculate the concentration increase due to the emission source, the instruments were assigned the up- or downwind position according to the dominant wind direction for each 30-min period.

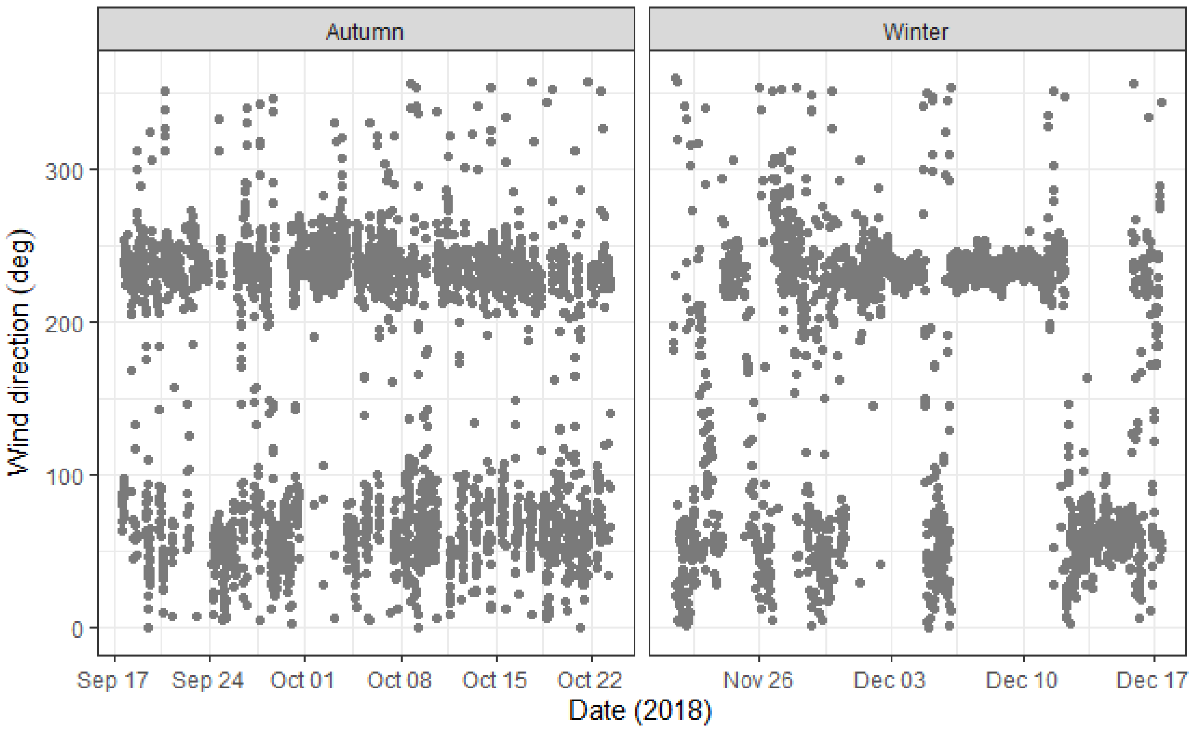

Figure SI1.3. Wind directions for each 30-min averaging period at the dairy housing during both measurement campaigns.

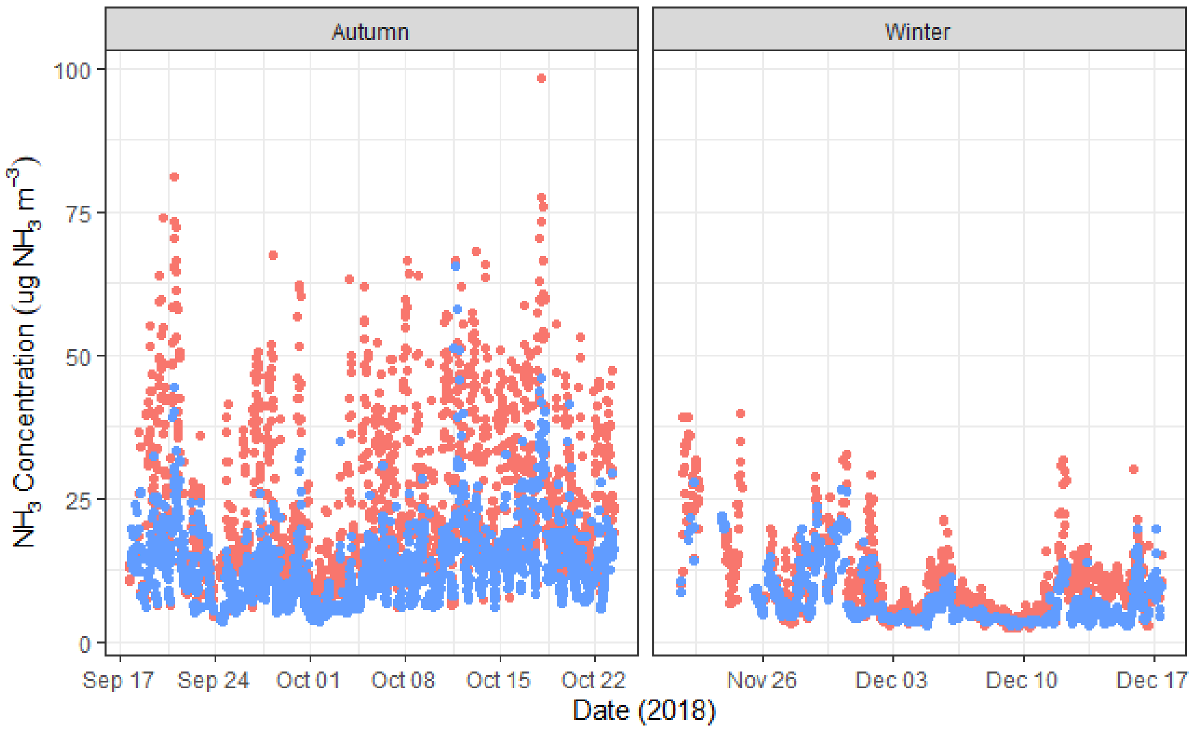

Figure SI1.4. Raw (unfiltered by micrometeorological conditions) 30-min NH_3 concentration data of the upwind background (blue) and downwind plume (red) levels.

SI1.2 Correlation statistics

Correlations of NH_3 emissions with environmental conditions by measurement period and wind direction are summarized in Table SI1.1.

Table SI2.1 Correlation statistics of NH_3 emissions with environmental variables at the dairy housing.

Time offset (h)	*Measurement period*	*Wind direction*	*Temperature*		*Wind speed*	
			coefficient r	*p - value*	*coefficient r*	*p - value*
0	*Autumn*	SW	0.07	0.62	0.005	0.96
		NE	0.14	0.18	0.33	<0.001***
		all	0.27	<0.001***	0.27	<0.001***
	Winter	SW	0.16	0.06	-0.01	0.83
		NE	0.42	<0.01**	0.13	0.18
		all	0.06	0.37	-0.03	0.62
	all	all	0.51	<0.001***	-0.18	<0.001***
1-2	*Autumn*	SW	0.28	<0.01**	0.08	0.4
		NE	0.24	<0.01**	0.37	<0.001***
		all	0.33	<0.001***	0.30	<0.001***
	Winter	SW	0.31	<0.001***	-0.06	0.35

		NE	0.26	<0.01**	-0.03	0.70
		all	0.21	<0.001***	-0.06	0.25
	all	all	0.55	<0.001***	-0.20	<0.001***

Statistically significant correlations are marked with * for p <0.05, ** for p <0.01, and *** for p <0.001.

SI1.3 Wind direction dependencies of emissions

The winds were more dominant from the NE during autumn and from the SW during winter (Figure SI1.5).

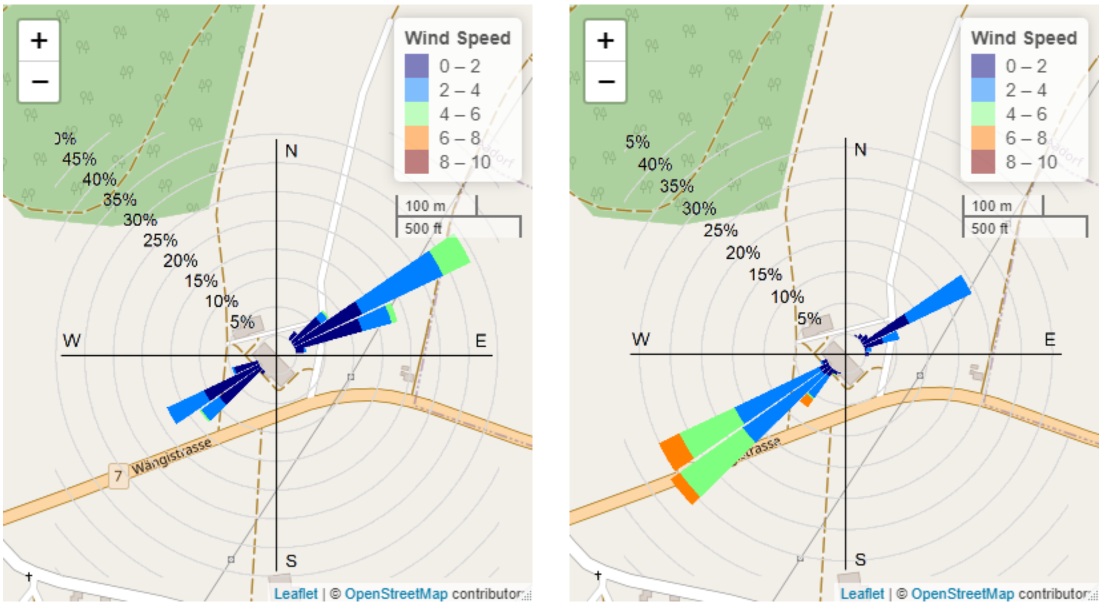

Figure SI1.5. Wind roses superimposed on the site map showing the wind speed frequency by wind direction for the autumn (left) and winter (right) measurement periods at the dairy housing. Map data © OpenStreetMap contributors.

Daily profiles of NH_3 emissions and correlations with friction velocity $u*$ are shown in Figure SI1.6 with approx. 20% higher emissions with NE winds during autumn, which also showed slightly higher correlations.

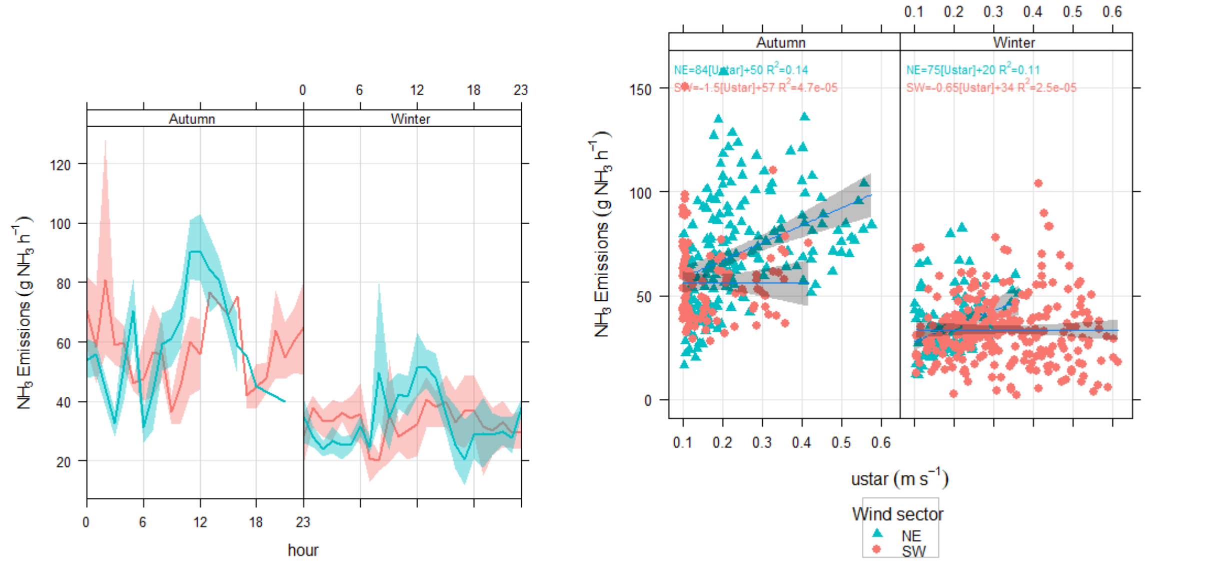

Figure SI1.6 Mean diel NH_3 emissions (left) separated by sector (red SW, blue NE) and correlated with friction velocity *u** (right) with linear regressions and coefficients for each wind direction and measurement period at the dairy housing.

SI2. Wastewater treatment plant

SI2.1 Supplementary data

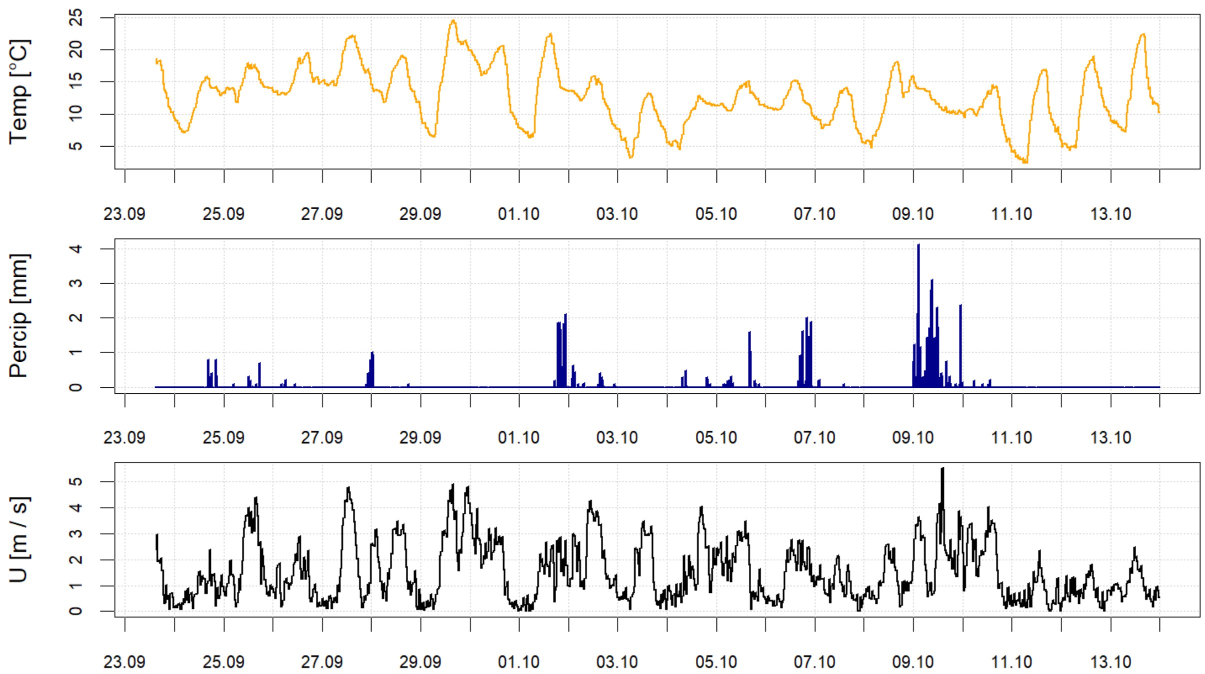

Figure SI2.1. Meteorological conditions (temperature, precipitation, and wind speed) recorded on site during the measurements at the WWTP. Reproduced from the supplemental information in Bühler et al. (2022).

Operational parameters and conditions at the WWTP during the measurement period are shown in Table SI2.1 and bLS weightings for each emitting structure at the WWTP are given in Table SI2.2. The WWTP had a total digester volume of 2200 m^3, and 1960 m^3 for the sludge storage tanks (surface of 331 m^2), of which 632 m^3 were in use during the measurement period. Measured concentrations by the up- and downwind miniDOAS instruments, as well as the wind directions at the WWTP are shown in Figures SI2.2 and 2.3.

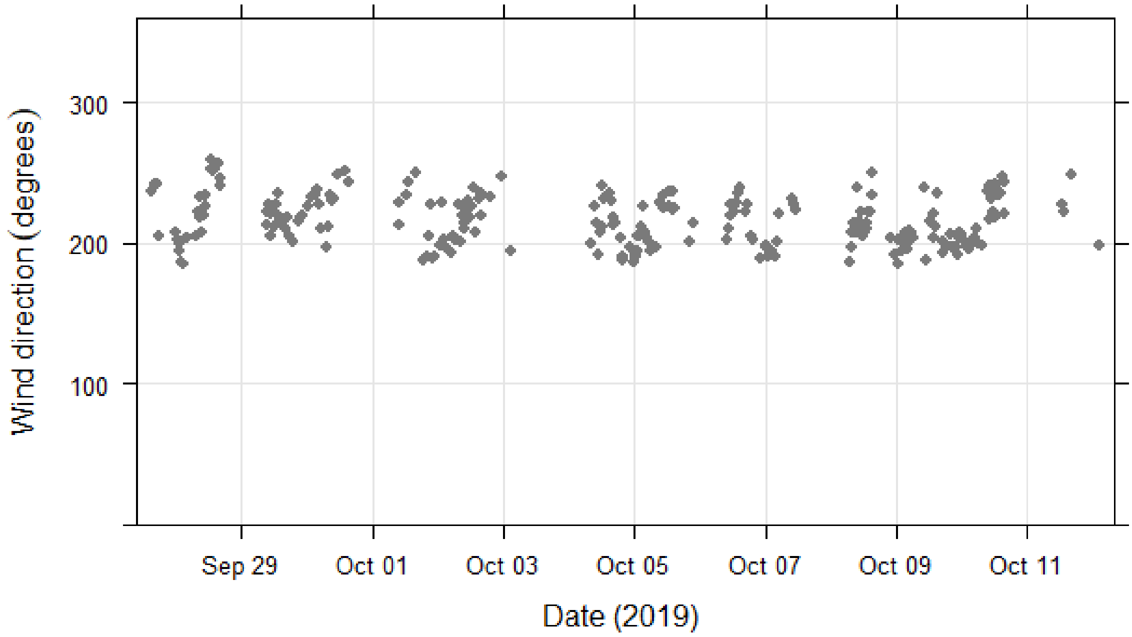

Figure SI2.2 Wind directions for the instrument placements up- and downwind of the WWTP after filtering for valid measurement conditions.

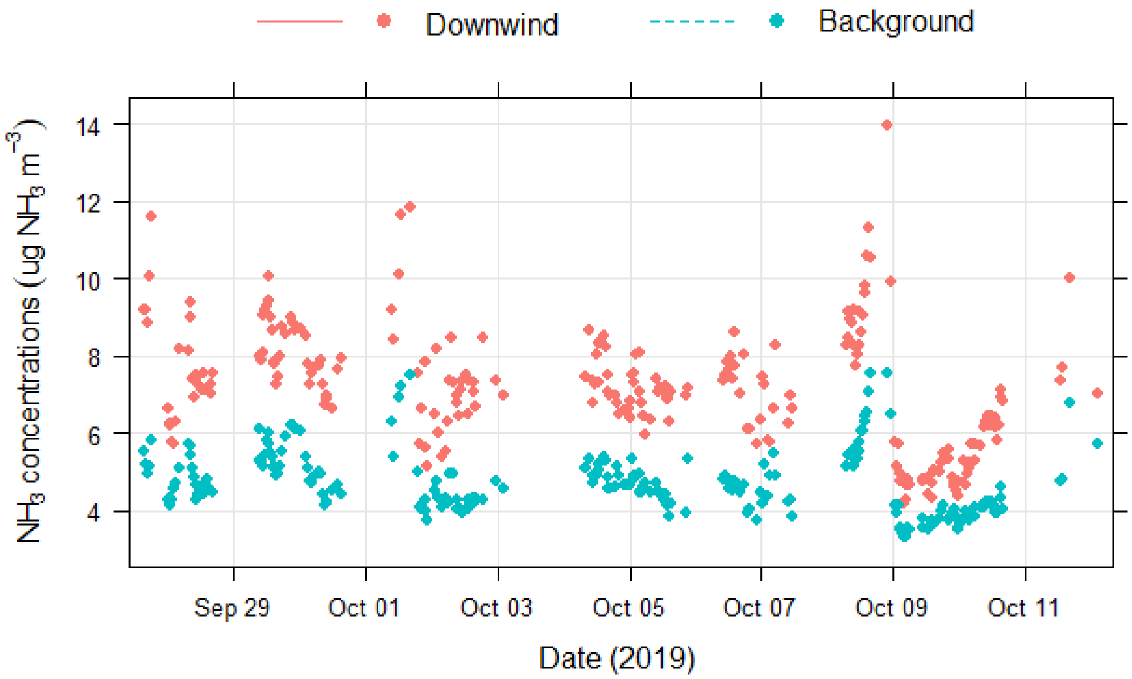

Figure SI2.3 Filtered ammonia concentrations for valid conditions measured by the miniDOAS instruments placed up- (blue) and downwind (red) of the emission source at the WWTP.

SI2.2 Operational data and statistics

Table SI2.1 Mean operational conditions at the wastewater treatment plant during the measurement period.

Parameter	*Units*	*Mean*	*Median*	*SD*	*Min*	*Max*
Inflow pH		7.39	7.39	0.23	6.79	7.93
Temperature	°C	17.7	18.0	1.3	15.3	20.
Dry matter (fresh sludge)	%	5.46	5.34	0.76	3.52	6.72
Inflow rate	L s^{-1}	141	118	54	91	314
Inflow volume	m^3 d^{-1}	11168	9380	6497	7829	30660
NH_4-N (inflow)	mg l^{-1}	33.1	36.2	8.67	15.7	42.3
NH_4-N (outflow)	mg l^{-1}	0.09	0.05	0.14	0.02	0.52
Total NH_4-N flow	kg d^{-1}	336	341	233	230	1034
COD* concentration	g l^{-1}	299	310	42	156	424
COD* Flow	kg d^{-1}	2862	2933	1090	1866	6133

*COD: Chemical Oxygen Demand

Table SI2.2 Weightings applied to the emission of the different source structures at the wastewater treatment plant.

Structure	*Weighting**	***Reference***

Storage tanks	0.81	Kupper et al., 2020
Sand trap	0.1	Samuelsson et al., 2018
Digester	0.4	Samuelsson et al., 2018
Primary clarifier	0.04	Samuelsson et al., 2018
Secondary clarifier	0.004	Samuelsson et al., 2018
Aeration tanks	0.006	Samuelsson et al., 2018

*Weightings are calculated as fractions from emission factors for each source area, which were based on values from the literature.

Table SI2.3 summarises correlations of NH_3 emissions with different driver variables using a synchronous correlation, as well as lagged correlations, whereby a positive lag indicates that the predictor variable lags behind the NH_3 emissions, while a negative lag shows that it precedes changes in emissions. The lagged correlations are only presented if they were higher than the synchronous correlation and only the lag with the maximum offset correlation is shown.

Table SI2.3 Correlations of predictor variables for NH_3 emissions at the WWTP.

Parameter	*Time offset (h)*	*Correlation coefficient*	*p-value*
Air temperature	0	0.48	<0.001***
	+3	0.75	<0.001***
pH	0	0.15	0.022*
	-4	0.53	<0.001***
Sludge tank agitation	0	-0.11	0.088
	-4	-0.19	0.002**
	+4	0.33	<0.001***
Incoming solar radiation	0	0.68	<0.001***

Statistically significant correlations are marked with * for $p < 0.05$, ** for $p < 0.01$, and *** for $p < 0.001$.